2. Vehicles can be designed to provide crash protection to the occupant at little or no penalty to the weight and cost of the vehicle.

3. Vehicle crashworthiness can be improved by providing the design principles to designers and by emphasizing the importance of this aspect of design responsibility. Decisions and design choices can then be influenced and in cases where two or more comparable choices are possible, the choice in favor of improved crashworthiness can be made.

4. Overall vehicle structural crashworthiness requires design for crash loads with an objective of maintaining a protective envelope around the occupant and reducing the crash loads transmitted to him by controlled deformation of surrounding structure.

5. Seating and restraint systems should be designed to provide adequate restraint in all loading directions and to minimize decelerative loading of the occupant.

6. Seating and restraint systems should have the strength required to remain in place until the surrounding structure collapses.

7. Some analytical procedures are available and some are being developed which can be used to evaluate and optimize structures and subsystems for occupant survival. Additional tools are needed to enable overall systems to be optimized for both structural crashworthiness and mission performance.

8. Creative innovation is needed to develop structural design components and concepts that can provide the stiffness and strength needed to perform the primary design function, but that will efficiently and progressively deform with fracture during crash loading.

References

1. Turnbow, J. W. *et al.*, "Crash Survival Design Guide," Dynamic Science, USAAVLABS Tech. Rep. 70-22, U.S. Army Aviation Mater. Lab.,* Fort Eustis, Virginia (1971) (latest edition to be published).
2. Haley, J. L., "Analysis of Existing Helicopter Structures to Determine Direct Impact Survival Problems," U.S. Army Board for Aviation Accident Res., Fort Rucker, Alabama (1971).
3. "Crash Injury Investigation, S-2B Snow Aerial Applicator Aircraft Accident," Aviation Crash Injury Res., Phoenix, Arizona (October 18, 1961).
4. Bruggink, G. M. *et al.*, "Injury Reduction Trends in Agricultural Aviation," *Aerospace Med.* **35**, No. 5 (1969).
5. "Crash Survival Investigation Textbook," Dynamic Sci., A Division of Marshall Ind., The "AvSER" Facility, 1800 W. Deer Valley Drive, Phoenix, Arizona (October 1968).
6. Gatlin, C. I. *et al.*, "Analysis of Helicopter Structural Crashworthiness," Volumes I and II, USAAVLABS Tech. Reps. 70-71A and 70-71B. U.S. Army Air Mobility Res. and Develop. Lab., Fort Eustis, Virginia, AD 880 680 and AD 880 678 (January 1971).

* Now U.S. Army Air Mobility Res. and Develop. Lab.

J. R. Rice and D. M. Tracey, "Computational Fracture Mechanics", in Numerical and Computer Methods in Structural Mechanics (eds. S. J. Fenves et al.), Academic Press, N.Y., 1973, pp. 585-623.

Computational Fracture Mechanics

J. R. Rice and D. M. Tracey

BROWN UNIVERSITY
PROVIDENCE, RHODE ISLAND

Some areas of fracture mechanics which are being developed through computational stress analysis methods are surveyed. These include the numerical determination of elastic stress–intensity factors, the elastic–plastic analysis of near crack deformation fields, three-dimensional analysis of cracked bodies, and the description of fracture mechanisms on the micro-scale.

In addition, finite-element procedures are presented for the accurate numerical determination of elastic–plastic fields in the immediate vicinity of a crack tip. These are based on asymptotic studies of crack tip singularities in plastic materials, the results of which are summarized here and further extended for the nonhardening case. A new finite-element is presented which allows the requisite crack tip opening and associated $1/r$ shear strain singularity for this case, but with strictly nonsingular dilatation. This is employed in the elastic–perfectly-plastic solutions for small-scale plane strain yielding at a crack tip, and for yielding from small scale to limit load conditions in a circumferentially cracked round bar. Resulting numerical solutions are shown to be in excellent accord with analytical predictions, and parameters of the near tip field of interest in developing a fracture criterion are discussed.

1. Introduction

Current fracture mechanics research is focused in two principal directions: the development of phenomenological explanations of crack extension behaviors, and the description of micromechanical processes of material separation on the microscale. Both have come to rely strongly on computational methods of stress analysis.

In the first, the goal is to correlate crack extension behavior in subcritical growth by fatigue or stress corrosion, or in critical growth due to an overload, in terms of parameters from analytical solutions which characterize the near tip stress field. Elastic fracture mechanics is a case in point: When the crack extension behavior of interest is accompanied by a small crack-tip plastic zone, in comparison to crack depth and uncracked dimensions of a flawed specimen or structure, the correlation is in terms of the elastic stress–intensity factor. This is the coefficient of the inverse square root crack tip singularity in an elastic stress field. It serves to characterize the influence of applied loads and flaw geometry on the near tip field for such small scale yielding conditions, even though the predicted elastic stress field is wrong in detail within the plastic region.

Hence the analytical problem in elastic fracture mechanics is to determine the stress–intensity factor. Several numerical methods have been developed for this, including boundary collocation, numerical solution of integral equations, and finite elements. There is now a substantial literature which we shall review briefly here.

Plasticity effects limit this approach, and there is much current work on attempting to define and make use of parameters from elastic–plastic solutions which might similarly characterize the near crack tip field. This regime must be understood not only to deal with flawed structures failing under large scale yielding conditions, but also to allow fracture test results on small (and hence often fully plastic) precracked laboratory specimens to be accurately interpreted for assessing the safety of a flawed structure under nominally elastic conditions. Analysis in this elastic–plastic range is based principally on finite-element methods. These must, however, reveal sufficient detail on a fine scale at the crack tip, and for this reason it is necessary to take special precautions in the design of near tip finite elements.

Our approach is based on using asymptotic studies of elastic–plastic crack tip singularities as a guide to the development of displacement assumptions within elements. Previous investigations of this type are reviewed, and a new finite-element is described which allows the $1/r$ shear-strain singularity appropriate to the nonhardening idealization. Application of this element to the plane-strain small-scale yielding problem and to the circumferentially cracked round bar problem leads to highly accurate descriptions of the near tip field, and these may be useful in a phenomenological assessment of counterparts to the elastic stress–intensity factor in correlating fracture behavior.

There is, however, no single parameter which can uniquely characterize the near crack tip field in the large-scale yielding range, especially when prior stable crack advance under increasing load must be considered. Hence studies of fracture on the microscale are of significance not only for basic understanding and as guides to alloy design, but also for suggesting suitable crack extension criteria to employ in flaw stress analysis and test correlations at the macroscopic level. Very much remains to be done in clarifying the mechanics of separation processes on the microscale, and in merging models at this level with macroscopic crack stress analysis for fracture prediction. We discuss the work to date in these areas and point out some of the challenging computational problems of plastic deformation, finite strain, and instability which appear at the microstructural level.

Our paper is divided into sections on the numerical determination of elastic stress–intensity factors in two-dimensional problems; crack tip plasticity, singular finite-element formulations, and results; three-dimensional crack problems, especially surface flaws; and fracture mechanics problems on the microscale. For a general background on analytical aspects of the subject, the reader may wish to consult the review papers by Paris and Sih [1], Rice [2], and McClintock [3].

2. Numerical Determination of Elastic Stress Intensity Factors (Two-Dimensional Problems)

The stress field at the tip of a sharp crack in an isotropic, linear, elastic material under loading conditions symmetric about the crack surface (Mode I) contains a stress singularity of the form

$$
\begin{aligned}
\sigma_{rr} + \sigma_{\theta\theta} &\to 2K(2\pi r)^{-1/2}\cos(\theta/2) \\
\sigma_{zz} &\to 2\nu K(2\pi r)^{-1/2}\cos(\theta/2) \\
\sigma_{\theta\theta} - \sigma_{rr} + 2i\sigma_{r\theta} &\to iK(2\pi r)^{-1/2}\sin(\theta)e^{i\theta/2}
\end{aligned}
\tag{1}
$$

where (r, θ, z) is a cylindrical polar system with origin lying at the point of interest along the crack front, with the z direction parallel to the crack tip, and with $\theta = \pm\pi$ on the crack surfaces (see Fig. 1). Here i is the unit imaginary number, and K is the stress–intensity factor. This same stress distribution with $\sigma_{zz} = 0$ applies to thickness averages in the simplest two-dimensional theory of generalized plane stress. The intensity factor is the parameter on which elastic fracture mechanics is based, and hence there is considerable interest in its numerical determination. We review some numerical methods for determining K here for two-dimensional problems of plane strain and

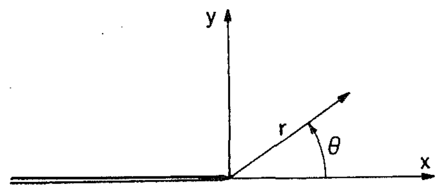

Fig. 1. Coordinates for description of near tip stress states.

generalized plane stress. Three-dimensional problems are discussed in a subsequent section.

The numerical methods may be divided broadly into those based on analytical representations of solutions (principally through analytic function theory) and those based on finite-element methods. Some of the former are limited as to the class of problems which may be handled, whereas the usual accuracy problems near singularities arise with the latter, and must be circumvented.

2.1. Boundary Collocation

Muskhelishvili's stress functions take the form [2]

$$\phi'(\zeta) = \zeta^{-1/2} f(\zeta) + g(\zeta) \tag{2}$$
$$\psi'(\zeta) = -\phi'(\zeta) - \zeta\phi''(\zeta) + \zeta^{-1/2} f(\zeta) - g(\zeta)$$

for a single straight Mode I crack penetrating in from the boundary of a body, where $\zeta = re^{i\theta} = x + iy$ and where the functions f and g are analytic everywhere within the body, including points along the crack line. For an internal Mode I crack of length l, the same form applies with $\zeta^{-1/2}f(\zeta)$ replaced by $\zeta^{-1/2}(\zeta + l)^{-1/2}F(\zeta)$, where $F(\zeta)$ is again analytic everywhere within the body, including the crack line. It is rigorously true that f (or F) and g have expansions of the form

$$f = \sum_0^\infty a_n \zeta^n, \qquad g = \sum_0^\infty b_n \zeta^n \tag{3}$$

where a_0 is expressible as $(8\pi)^{-1/2}K$, which converge in a neighborhood of the crack tip up to a radius equal at least to that of the nearest portion of external boundary, or of some other singularity of the problem.

The boundary collocation method as employed by Gross *et al.* [4–6] for edge cracks, and in the modified form by Kobayashi *et al.* [7] for an internal crack, in rectangular specimens adopts truncated power series in ζ for f and g. These are assumed to apply everywhere within the body, and the coefficients are chosen to match imposed stress conditions at discrete points of the external boundary. Commonly an excess number of collocation points are

chosen so that an overdetermined system is obtained which is then solved in the sense of obtaining a least square minimization of the total error over the discrete points.

The method is attractive because it automatically satisfies traction-free boundary conditions on the crack surfaces. There does remain, however, a question in need of resolution as to the limitations set by the limited radius of convergence of complete power series for f and g.

2.2. Approximate Conformal Mapping

Another general method that has been used to obtain crack solutions is that of approximate conformal mapping, which may be applied to cracks emanating from holes in infinite bodies or to edge cracks in simply connected bodies. The technique involves finding accurate polynomial approximations to the mapping function which transforms the physical cracked domain into a circular region. The motivation to mapping is the fact that if a map of the form of a polynomial or ratio of polynomials is available, the stress functions expressed in terms of the auxiliary plane complex spatial variable can be obtained exactly by solving a finite system of equations. Bowie [8–10] treated the problem of an isolated circular hole with radial cracks and edge-notched strips using this method. Kaminskij [11] considered the case of isolated elliptical holes weakened by edge cracks. The stress–intensity factor may be unambiguously defined if the approximate polynomial mapping is chosen to keep the crack tip sharp (as may be done, whereas other types of corners must be rounded by such an approximation).

Bowie and Neal [12] have used a hybrid mapping, collocation technique to treat the doubly connected circular disk with an internal crack. The procedure is to choose a simple function which maps a circle and its exterior onto the crack and its exterior. Truncated series for the stress functions in the auxiliary plane are chosen with the coefficients determined by collocating on the mapped external boundary. Along with stress and displacement, force and moment boundary values are used in the collocation.

2.3. Integral Equations

A crack may be represented as a continuous distribution of dislocations. Rice [2] has outlined a method whereby the solution for an isolated dislocation in a body may be used to generate a singular integral equation governing the crack problem, and has shown how the equation is reduced to a regular Fredholm equation which may be solved numerically in a straightforward fashion. Related methods have been employed by Grief and Sanders [13] for a stringer reinforcement on a cracked plate and by Bueckner [14] for edge cracks.

More generally, solutions to plane elasticity problems may be given in the form of integrals, taken around the boundary, of fundamental singularities times unknown weighting functions, with the resulting singular integral equations being solved numerically. Cruse [15] and Cruse and Van Buren [16] have made effective use of this method for the numerical solution of three-dimensional elastic-crack problems; no results seem yet to be available on the application of the method to plane problems. Tirosh [17] has solved some crack problems for Mode III (antiplane strain) deformation through a related technique, but with an important modification which assures crack tip accuracy: For the fundamental singularity he chooses the field of an isolated dislocation in an infinite body with a semi-infinite crack. This automatically leaves the crack surfaces traction free, and one has to deal only with an integral equation along the external portion of the boundary.

2.4. Finite-Element Methods

The usual failure of numerical methods near singularities such as a crack tip requires either the use of special crack-tip finite-elements which embed the inverse square root singularity or, if standard elements with polynomial interpolation functions are used, the use of indirect procedures such as extrapolation to the tip or energy release methods.

Chan *et al.* [18] discussed extrapolation methods of determining K from constant stress triangular elements. The procedure is to plot the product of $r^{1/2}$ with some stress component (say $\sigma_{\theta\theta}$), as a function of distance along some ray emanating from the tip, and to extrapolate this as a smooth curve to the tip so as to estimate K. The result is, of course, generally quite different from the value which would be estimated based on stresses in the elements nearest the tip. Alternatively, the exptrapolation may be based on a product of $r^{-1/2}$ with a displacement, making use of the known displacements associated with the stress singularity (e.g. Rice [2])

$$u_x + iu_y = K/2G(r/2\pi)^{1/2}(\kappa - \cos\theta)e^{i\theta/2} \tag{4}$$

Here G is the shear modulus, and $\kappa = 3 - 4\nu$ for plane strain, or $(3 - \nu)/(1 + \nu)$ for plane stress, where ν is Poisson's ratio. Chan *et al.* reported an agreement within 4–5% of known solutions for K, when approximately 2000 degrees of freedom were used, by using extrapolations based on $\sigma_{\theta\theta}$ directly ahead of the tip or on u_y along the crack surface.

Alternatively, K can be determined from a calculation of the decrease in potential energy of a body due to an increase in crack length, with applied loads and displacement constraints remaining fixed. For plane strain the relation between K and the energy release rate dP/dl is given by

$$dP/dl = -(1 - \nu^2)K^2/E \tag{5}$$

Hayes [19] used this method in treating a variety of configurations with simple triangular elements to obtain about 5% accuracy when 1000 degrees of freedom were allowed. His program was written to change the crack length automatically after a solution, by successively canceling reaction forces on nodes ahead of the crack. His use of an overrelaxation equation solver made this an efficient scheme, since the master stiffness matrix is only slightly perturbed in the process.

A related method discussed by Chan *et al.* [18] calculates the energy release rate without the necessity of actually re-solving a new problem for a slightly extended crack. This is done through Rice's J integral [20]:

$$J = \int_\Gamma [(W - \sigma_{xx}\,\partial u_x/\partial x - \sigma_{xy}\,\partial u_y/\partial x)\,dy + (\sigma_{yx}\,\partial u_x/\partial x + \sigma_{yy}\,\partial u_y/\partial x)\,dx] \tag{6}$$

Here W is the elastic strain-energy density ($=\frac{1}{2}\sigma_{ij}\varepsilon_{ij}$ for a linear material) and the path Γ on which the integral is taken is an arbitrarily chosen contour beginning at any point on the lower crack surface of Fig. 1, encircling the tip, and ending at any point on the upper crack surface. The integral has a value which is independent of the particular path chosen; there is no restriction that the material be *linear* elastic, but instead only that its stress–strain relations be consistent with the existence of a strain-energy function (i.e., $\sigma_{ij}\,d\varepsilon_{ij} = dW$, an exact differential). The physical interpretation of J is as the energy release rate [2, 20], and hence in the case of a linear elastic material

$$J = (1 - \nu^2)K^2/E \tag{7}$$

Chan *et al.* chose an integration path Γ for the integral lying far from the tip and coinciding with the boundary of their edge-cracked specimen. Resulting values of K, obtained through evaluating the integral from the triangular finite-element solution, were reported to have an accuracy essentially similar to that of the extrapolation method.

Other methods of solving for K have been discussed by Barone and Robinson [21] and Rice [22]. These methods use elastic reciprocity properties to formulate new boundary-value problems whose solution leads to a determination of K, but through calculations which do not require numerical accuracy in the near tip region.

The alternative to the preceding methods is that of directly embedding the elastic singular term in the displacement assumption for the near tip finite elements. Wilson [23] developed an axisymmetric ring element of circular cross section centered at the crack tip for investigation of the circumferentially cracked round bar under torsion. The stiffness of the element was formed by integrating the strain-energy density of the dominant $r^{-1/2}$ singularity over the circular cross section of the element. Conventional triangular ring elements covered the remainder of the mesh. The undetermined parameters in the formulation were K and the displacements of nodes not lying on the crack-tip element boundary. The same procedure is applicable to tension, and Hilton and Hutchinson [24] have followed a similar procedure in obtaining deformation plasticity solutions for cracks under in-plane deformation. Tracey [25] used a mesh composed of isosceles trapezoidal-shaped elements focused into the crack tip. The elements nearest to the tip had a $r^{1/2}$ variation of displacement specified, while the adjacent elements were treated as ordinary isoparametric elements. The near-tip interpolation function was designed to guarantee interelement displacement continuity. More details of this will be given in the section presenting our elastic–plastic numerical results.

3. Crack Tip Plasticity

As we have noted, studies on crack-tip plasticity are important for extension of the phenomenological fracture mechanics approach to the large-scale yielding range, and also for setting boundary conditions on models of microscale separation mechanisms at the crack tip. In both cases, rather detailed descriptions of stress and deformation on a size scale that is small compared to overall plastic region dimensions seem to be required. Lee and Kobayashi [27], Marcal and King [28], Swedlow and co-workers [29, 30], Wells [31], and others have presented finite-element solutions for yielding near cracks or sharp-tipped notches, and much has been learned from these concerning the growth and shape of the plastic region and transitional behavior from the elastic to fully plastic ranges.

However, we think it unrealistic to expect that standard finite-element methods will give the detailed results desired in the near-tip region, as will be more apparent with the ensuing discussion. For this reason, our own computational work has relied heavily on a merging of computer methods with what is known from asymptotic studies of crack tip singularities in plastic materials. Here we refer specifically to the papers of Cherepanov [32], Hutchinson [33, 34], Rice [2, 20, 35], and Rice and Rosengren [36], which have elucidated the structure of plane-strain and plane-stress singularities at crack tips, both for materials idealized as nonhardening and for power law strain hardening materials [i.e., (stress) $\propto$ (strain)^N in the plastic range]. Indeed, approximate small-scale yielding solutions have been given [20, 33, 34, 36] for these cases on the basis of a deformation plasticity formulation and the J integral. Previous papers by Hilton and Hutchinson [24] and Levy *et al.* [37] have made similar use of the asymptotic studies in finite-element analyses. The first of these introduced a circular near-tip element in which the dominant power-law-hardening singularity strain and displacement distribution is assumed, but with an unknown amplitude. Levy *et al.* introduced a different type of singular element, which we shall describe later; our work is a continuation and refinement of that method.

Nearly all the results of the asymptotic studies and computational treatments have been for stationary cracks, and one of the major unresolved problems of the field is in clarifying the elastic–plastic mechanics of quasi-static crack advance. McClintock [3, 38] and Rice [2] have discussed this type of problem, for which the history-dependent nature of plastic stress–strain relations and the feature of crack advance into previously deformed material lead to near-tip strain distributions which are very different from those for stationary cracks. For example, Rice [20] has shown that a $1/r$ shear strain singularity results in the regions above and below the tip of a *stationary* plane strain crack in a perfectly plastic material, whereas McClintock [38] showed that nonsingular strains result in the case of a continuously advancing crack in a *rigid*–perfectly-plastic material under increasing imposed displacements at its boundary, and Rice [2] showed that a logarithmic strain singularity resulted at the tip for conditions of steady-state crack advance in an *elastic*–perfectly-plastic material. This is an area in which much remains to be done toward developing computational accuracy paralleling that now attainable for the stationary crack case, and analyses of this type are of obvious importance for a correlation of fracture tests in which substantial stable crack extension precedes the running crack instability (e.g., cracks in thin, ductile sheets). On the other hand, the stationary crack model alone seems appropriate for the abruptly initiated fractures which frequently result under conditions of plane strain constraint at the crack tip.

3.1. Crack-Tip Stress Field

The numerical solutions that we report in the next section are for stationary cracks under plane strain (or nearly so) conditions at the tip, and the material is idealized as isotropic and elastic–perfectly-plastic (of the Mises type). Large geometry change effects on the form of governing equations are neglected, although we shall consider these in the section on micromechanics. For these cases, Rice [2, 20] has given approximate arguments for validity of the stress state of the Prandtl slip line field (Fig. 2) in providing the limiting stress state as $r \to 0$ at the crack tip for cases of contained plastic yielding. Also, Hutchinson [34] and Rice and Rosengren [36] have noted that this field is the limit, as the hardening exponent N approaches zero, of their dominant singularity solutions for crack tip stresses. However, it cannot be expected that in this limit the "dominant singularity" does in fact dominate, as has been learned from the Mode III case, and indeed the Hutchinson–

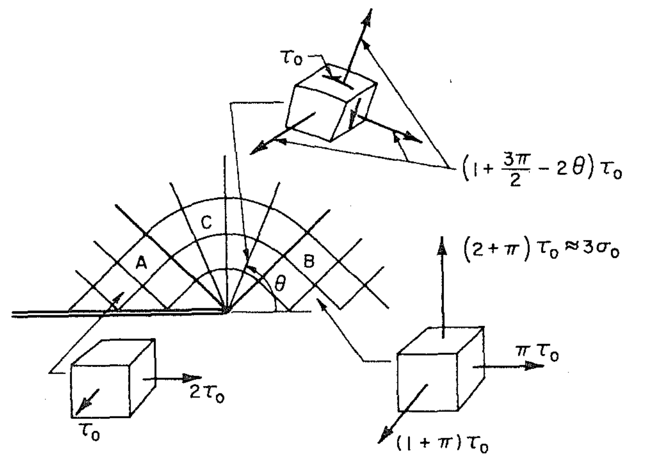

Fig. 2. Prandtl field as the limiting stress distribution as $r \to 0$, for contained plain strain yielding of a non-hardening material.

Rice–Rosengren equations have no unique solution for the strain distribution when $N = 0$.

Thus we reexamine the nature of the near crack tip field here both as motivation for our singular finite element formulation and as an extension of prior asymptotic studies of this type. In view of the boundedness of stresses in a nonhardening material it may be assumed that $r\,\partial\sigma_{ij}/\partial r \to 0$ as $r \to 0$, and hence the two stress equilibrium equations in polar coordinates take the form

$$\sigma_{rr} - \sigma_{\theta\theta} + \partial\sigma_{r\theta}/\partial\theta = 0, \qquad 2\sigma_{r\theta} + \partial\sigma_{\theta\theta}/\partial\theta = 0 \tag{8}$$

for the angular variation of the stress state at $r = 0$. The Mises yield condition $s_{ij}s_{ij} = 2\tau_0{}^2$, where s_{ij} is the stress deviator and τ_0 the yield stress in shear, and may be rewritten as

$$(\sigma_{rr} - \sigma_{\theta\theta})^2/4 + \sigma_{r\theta}^2 + (\sigma_{rr} + \sigma_{\theta\theta} - 2\sigma_{zz})^2/12 = \tau_0{}^2 \tag{9}$$

This is satisfied in any angular sector at the tip which is in the plastic state, and after differentiation with respect to θ and use of the equilibrium equations to simplify the result, we obtain (for $r = 0$)

$$6[\partial\sigma_{r\theta}/\partial\theta]\,[\partial(\sigma_{rr} + \sigma_{\theta\theta})/\partial\theta] = \partial[(\sigma_{rr} + \sigma_{\theta\theta} - 2\sigma_{zz})^2]/\partial\theta \tag{10}$$

By the flow rule for plastic strain increments,

$$\dot{\varepsilon}_{ij}^p = (\dot{\varepsilon}_{kl}^p\dot{\varepsilon}_{kl}^p/2)^{1/2}s_{ij}/\tau_0. \tag{11}$$

Thus, if there is a strain singularity at the tip in the angular sector under consideration, we must have $s_{zz} = 0$ there because conditions of plane strain prohibit a singularity in ε_{zz}^p. This means that

$$\sigma_{zz} = (\sigma_{rr} + \sigma_{\theta\theta})/2 \tag{12}$$

at $r = 0$ in such a sector. We may also note that this last equation would be valid for a rigid–plastic material, and that it would be approached as a limit for an elastic–plastic material subjected to monotonically increasing plastic deformations. Hence Eq. (12) is strictly valid in an angular sector where there is a strain singularity, and it would seem essentially correct even in angular sectors for which the plastic strains are nonsingular, although the argument cannot in general be made rigorous in sectors of the latter type.

With Eq. (12) the right side of Eq. (10) vanishes, and hence the stress state at $r = 0$ satisfies either

$$\text{(a)}\quad \partial\sigma_{r\theta}/\partial\theta = 0, \qquad \text{or} \qquad \text{(b)}\quad \partial(\sigma_{rr} + \sigma_{\theta\theta})/\partial\theta = 0. \tag{13}$$

In sectors for which (a) holds, the equilibrium equations and yield condition lead to stress states of the form

$$\sigma_{r\theta} = \pm\tau_0, \qquad \sigma_{rr} = \sigma_{\theta\theta} = \sigma_{zz} = \text{const} \pm 2\tau_0\theta \qquad \text{in (a) sectors} \tag{14}$$

Stress fields of this type which apply over a finite range of r are known as "centered fans" in slip line theory, and these appear above and below the crack tip in the Prandtl field of Fig. 2. In those sectors where (b) holds, one finds, as a consequence of the equilibrium equations, that

$$\sigma_{xx},\quad \sigma_{xy},\quad \sigma_{yy},\quad \sigma_{zz} \quad \text{are independent of } \theta \text{ in (b) sectors.} \tag{15}$$

That is, the stress components when referred to cartesian coordinates are constant at the tip in (b) sectors. These are known as "constant state" regions in slip line theory, and occur directly ahead of the tip and in regions adjacent to the crack surfaces for the Prandtl field.

Hence, to the extent that Eq. (12) holds, the stress distribution surrounding the crack tip over all angular ranges for which there is plastic yielding must be made up of centered fan sectors of type (a) and constant stress sectors of type (b). This holds for stationary as well as advancing cracks. If the entire angular range surrounding the crack tip is yielding, then the only possible stress distribution of this type, corresponding to a continuous stress variation with θ (as would be expected for problems of contained plastic yielding) and to symmetrical Mode I loading conditions, is that given by the Prandtl field of Fig. 2. Indeed, our computational results and those of Levy *et al.* [37] support this assertion of the Prandtl field as the limiting stress distribution as $r \to 0$ at least for problems of small scale contained yielding. However, it cannot be asserted a priori that Eqs. (13)–(15) govern in nonsingular plastic sectors.

Also, fully plastic flow fields of limit analysis may involve a variety of near tip stress distributions [2, 3], depending on overall geometry of the cracked specimen, and these may involve discontinuous stress distributions and nonyielding sectors, as well as discontinuous deformation concentration into shear bands emanating from the tip.

In comparison, Rice's [20] approximate treatment was based on simplifying the yield condition to the statement that the maximum in-plane shear stress is constant. This is the same as deleting the last term on the left in Eq. (9), so that Eq. (10) has zero on the right and thus Eqs. (13) and their consequences apply in *all* plastic sectors, whether singular or not. Within this approximation, all plastic sectors therefore consist either of centered fan or of constant stress regions. In the most general case, there may also be nonyielding sectors at the tip, although if the entire angular range is yielding and the stresses are continuous, then only the Prandtl field of Fig. 2 may result at $r = 0$. Note that when the Prandtl field is present the maximum tensile stress directly ahead of the tip is approximately $3\sigma_0$, where σ_0 is the tensile yield stress.

3.2. Displacements and Strain Singularity

We have remarked that near tip stress states, at least in singular regions, are familiar from slip line theory and indeed, for the approximation of the yield condition by the maximum in-plane shear criterion, slip line theory applies in all yielding regions. As Rice noted [20], a feature of a centered fan slip-line field at a stationary crack tip is that there is a nonunique displacement at the tip in the sense that a different displacement vector (u_x, u_y) results at $r = 0$ for each different ray of the fan along which the tip is approached. That is, the displacements at $r = 0$ vary with θ in the fan and hence there is a discrete opening displacement of the crack surfaces at the tip. Radial and circumferential lines are zero extension rate directions so that ε_{rr} and $\varepsilon_{\theta\theta}$ are nonsingular, the singular deformation consisting of a pure shear $\gamma_{r\theta}$ which becomes infinite as r^{-1}. Singularities result where slip lines focus to a point and thus the strain components are, in general, nonsingular in the constant stress sectors with a unique displacement resulting at $r = 0$ as the tip is approached through these sectors. There is also, however, a possibility of a sliding displacement discontinuity emanating from the tip along a slip line, and these frequently occur in limit flow fields [3]. The features of r^{-1} strain singularities, tip opening displacements, and lines of displacement discontinuity at limit load seem to be general features of crack tip fields in nonhardening materials, in the sense that they are also familiar from the Mode III case [3] and from the two-dimensional plane stress case [33, 34].

To study the near tip field in plane strain without recourse to its approximate representation in terms of slip lines, consider the polar coordinate strain

components

$$
\begin{aligned}
\varepsilon_{rr} &= \cos\theta\, \partial u_x/\partial r + \sin\theta\, \partial u_y/\partial r \\
\varepsilon_{\theta\theta} &= r^{-1}(-\sin\theta\, \partial u_x/\partial\theta + \cos\theta\, \partial u_y/\partial\theta) \qquad (16)\\
\gamma_{r\theta} &= r^{-1}(\cos\theta\, \partial u_x/\partial\theta + \sin\theta\, \partial u_y/\partial\theta) - \sin\theta\, \partial u_x/\partial r + \cos\theta\, \partial u_y/\partial r
\end{aligned}
$$

where it is convenient for this discussion to write the strain-displacement gradient relations as we have in terms of Cartesian displacements. We shall consider that the displacements may vary with θ at $r = 0$ and examine the restrictions placed on this variation by the flow rule. One does however expect bounded displacement components at the tip and thus it appears reasonable to assume that $r\, \partial u_i/\partial r \to 0$ as $r \to 0$.

Any plastic-strain singularity must conform to the incompressibility condition and since elastic strains are bounded we must therefore have $(\varepsilon_{rr} + \varepsilon_{\theta\theta})$ bounded at the tip. This means that $r(\varepsilon_{rr} + \varepsilon_{\theta\theta}) \to 0$ as $r \to 0$ and thus Eqs. (16) require that the displacements at $r = 0$ satisfy the constraint

$$\sin\theta\, \partial u_x{}^0/\partial\theta = \cos\theta\, \partial u_y{}^0/\partial\theta, \qquad (17)$$

where we use the notation $u_i{}^0(\theta)$ for $u_i(r, \theta)$ at $r = 0$. This same restriction applies also to displacement rates $\dot{u}_i{}^0$. We therefore have $r\varepsilon_{rr}$ and $r\varepsilon_{\theta\theta}$ both going to zero at the tip. On the other hand, it is seen from Eq. (16) that as $r \to 0$

$$
\begin{aligned}
r\gamma_{r\theta} \to \cos\theta\, \partial u_x{}^0/d\theta + \sin\theta\, \partial u_y{}^0/\partial\theta &= (\cos\theta)^{-1}\, \partial u_x{}^0/\partial\theta \\
&= (\sin\theta)^{-1}\, \partial u_y{}^0/\partial\theta \qquad (18)
\end{aligned}
$$

where the last two versions on the right follow from Eq. (17). Hence $\gamma_{r\theta}$ (or $\dot{\gamma}_{r\theta}$) exhibits a singularity of strength r^{-1} in any sector for which the crack tip displacements (or rates $\dot{u}_i{}^0$) vary with θ.

Recalling our previous study of the crack tip stress state, in which singular sectors were shown to be either of the centered fan [Eq. (14)] or constant stress [Eq. (15)] type, we see from the flow rule [Eq. (11)] that the stress state in a fan sector at a stationary crack tip is consistent with a singularity dominated by the polar shear rate $\dot{\gamma}_{r\theta}$, and the crack tip displacement rates may indeed vary with θ in such sectors. On the other hand, such a singularity violates the flow rule and hence is inadmissible in a constant stress sector. Crack tip displacement rates therefore cannot vary with θ in such sectors, with one exception: If the constant stress state of the sector is such that for some angle θ within it $\sigma_{r\theta} = \pm\tau_0$, then it is possible to have a discontinuity in $\dot{u}_i{}^0$ at that angle with $\partial\dot{u}_i{}^0/\partial\theta$ vanishing elsewhere. In this case the jump version of Eq. (17) applies across the discontinuity. It is in fact possible to view such a discontinuity as a centered fan sector with a vanishing angular range, since $\sigma_{r\theta} = \pm\tau_0$ at this angle.

It is of interest to note that while equilibrium considerations required singular sectors to be either of the fan or constant stress type, flow rule considerations show that only the former can in fact exhibit the $1/r$ singularity. Neighboring sectors *may* be of the constant stress type but this is not necessarily so, except for the maximum in-plane shear approximation to the yield condition.

Our finite-element formulation incorporates the preceding features of the near-tip field, in that we choose displacement assumptions which permit a variation with θ at the tip subject to the constraint of Eq. (17). This allows a direct calculation of the crack tip opening displacement, of the angular strength of the strain singularity, and of the tip stress state. Detail at this level is of course unattainable from conventional finite-element formulations.

For reporting our results we shall use the standard notation [2, 20] for the strain singularity, writing Eq. (18) in the form

$$\gamma_{r\theta} \rightarrow \frac{\tau_0}{G} \frac{R(\theta)}{r} \tag{19}$$

where τ_0/G is the initial yield strain in shear, and where the angular strength of the strain singularity is written so that $R(\theta)$ may be interpreted as an *approximate* measure of the linear extent of the plastically strained region at angle θ. From the preceding discussion, R (or more precisely, $\dot{R}$) is nonzero only in fan sectors. The function R is related to the displacement components, for by comparing Eqs. (18) and (19) we see that

$$\partial u_x{}^0/\partial\theta = (\tau_0/G)R\cos\theta, \qquad \partial u_y{}^0/\partial\theta = (\tau_0/G)R\sin\theta \tag{20}$$

Also, by integrating the last of these, the opening displacement between the upper and lower crack surfaces at the tip is

$$\delta_t = 2(\tau_0/G)\int_0^{\pi} R(\theta)\sin\theta\, d\theta \tag{21}$$

When the Prandtl field applies, the limits are the angular range $\pi/4$ to $3\pi/4$ of the fan sector.

If one adopts a deformation theory of plasticity, which models the material as if it were nonlinear elastic, then the J integral remains path independent for contours Γ passing through the plastic region provided that the appropriate W is used. Taking the Prandtl field as the near tip stress state and shrinking Γ to the tip, Rice [20] showed that J could be expressed as

$$J = (2\tau^2{}_0/G)\int_{\pi/4}^{3\pi/4} R(\theta)[\cos\theta + (1 + 3\pi/2 - 2\theta)\sin\theta]\, d\theta. \tag{22}$$

For small-scale yielding, J retains its linear elastic value of Eq. (7), and this serves as the basis for some approximations.

4. Singular Finite-Element Formulation and Results

Finite-element incremental elastic–plastic solutions to the small-scale-yielding plane-strain problem and the large-scale-yielding of a circumferentially cracked tension bar are described in this section. As has been emphasized, the goal is to obtain reliable results at the crack tip singularity as well as globally. These nonlinear problems are linearized by specifying the load in small, finite steps and solving for the resulting deformation at each step by the tangent modulus approach. Within each increment an iterative scheme is adopted which allows convergence to the best representative constitutive matrices of yielded elements for the increment. The scheme is outlined here for the isotropic, perfectly plastic Mises material idealization; it could also serve as the basis for treatment of more general cases.

4.1. Iterative Procedure

To illustrate the procedure consider $\mathbf{s}^0$ as the deviatoric stress vector of an element at the beginning of a particular load increment. To remain general let $\mathbf{s}^0$ lie inside the yield surface. Estimate that the strain increment due to the current load increment is parallel to that of the solution for the previous load increment, and scaled according to increment size. Considering this estimate to be entirely elastic, calculate the corresponding fictitious final stress $\mathbf{s}^2$ ($=\mathbf{s}^0 + 2G\Delta\mathbf{e}^{\text{est}}$, where G is the elastic shear modulus and $\Delta\mathbf{e}^{\text{est}}$ is the deviatoric part of the strain increment estimate). Figure 3 is a π-plane

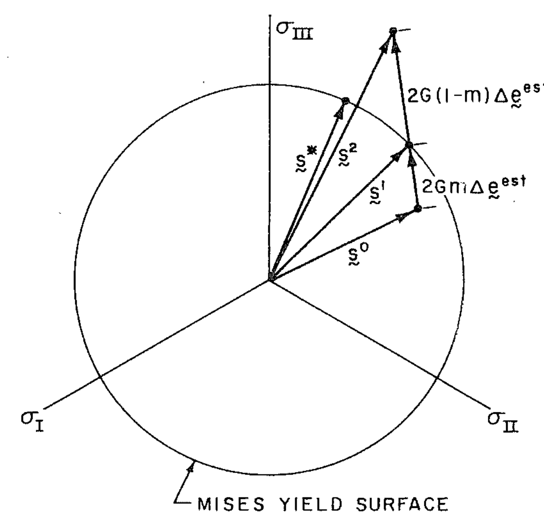

Fig. 3. π-plane view of stress states of an element during a load increment.

projection of the stress vectors and the Mises yield surface, which appears as a circle of radius $\sqrt{2}\tau_0$ in this plane. The material would yield at $\mathbf{s}^1$. For this case of transition from elastic to elastic–plastic behavior within an increment the partial-stiffness approach of Marcal and King [28] is followed. The matrix $\mathbf{D}$ which relates deviatoric stress increment to deviatoric strain increment is divided into elastic and elastic–plastic portions according to the ratio $m = |s^1 - s^0|/|s^2 - s^0|$:

$$\mathbf{D} = m\mathbf{D}^{\mathrm{el}} + (1 - m)\mathbf{D}^{\mathrm{el-pl}} \tag{21}$$

$\mathbf{D}^{\mathrm{el}}$ is the diagonal matrix $2G\mathbf{I}$ and $\mathbf{D}^{\mathrm{el-pl}}$ is equal to $2G(\mathbf{I} - \mathbf{nn}^{\mathrm{T}})$, where $\mathbf{n}$ is the unit vector $\mathbf{s}/\sqrt{2}\tau_0$ normal to the yield surface at the stress state $\mathbf{s}$.

Previous analyses [27, 28] have used the unit normal vector $\mathbf{n}^1$ at the initial yield state $\mathbf{s}^1$ to define $\mathbf{D}^{\mathrm{el-pl}}$ for the increment. This corresponds to a simple Euler integration of the actual constitutive "rate" equation over the elastic–plastic portion of the increment. The large-load step sizes which are necessary for computational economy for some problems make this an unacceptable approximation due to the associated large stress increments at each step. Hayes [19] specified $\mathbf{D}^{\mathrm{el-pl}}$ for the increment by using the unit vector in the direction of the estimated average stress vector predicted by the Marcal–King procedure,

$$\mathbf{s}^1 + G(\mathbf{I} - \mathbf{n}^1\mathbf{n}^{1\mathrm{T}})(1 - m)\,\Delta\mathbf{e}^{\mathrm{est}}$$

In the present scheme we use the unit vector $\bar{\mathbf{n}}$ in the direction of the average of $\mathbf{s}^1$ and $\mathbf{s}^2$,

$$\bar{\mathbf{n}} = \frac{\mathbf{s}^1 + \mathbf{s}^2}{|\mathbf{s}^1 + \mathbf{s}^2|} = \frac{\mathbf{s}^1 + G(1 - m)\,\Delta\mathbf{e}^{\mathrm{est}}}{|\mathbf{s}^1 + G(1 - m)\,\Delta\mathbf{e}^{\mathrm{est}}|} \tag{22}$$

because this has the remarkable feature that the corresponding $\mathbf{D}^{\mathrm{el-pl}}$ transforms $(1 - m)\,\Delta\mathbf{e}^{\mathrm{est}}$ to a stress increment which, when added to $\mathbf{s}^1$, results in a final stress $\mathbf{s}^*$ which precisely meets the yield criterion. The strain estimates are found to converge quite rapidly using this procedure so that the approximation within an increment is essentially the use of a secant between the initial and final stress states to define the yield surface during the increment.

To prove that the stress state $\mathbf{s}^*$ lies on the yield surface when $\bar{\mathbf{n}}$ is used to determine the plastic flow during the increment, we must prove that

$$\mathbf{s}^{*\mathrm{T}}\mathbf{s}^* - \mathbf{s}^{1\mathrm{T}}\mathbf{s}^1 = 0, \qquad \text{or} \qquad (\mathbf{s}^* + \mathbf{s}^1)^{\mathrm{T}}(\mathbf{s}^* - \mathbf{s}^1) = 0 \tag{23}$$

Equation (23) is proved by demonstrating the orthogonality of the vectors $(\mathbf{s}^* + \mathbf{s}^1)$ and $(\mathbf{s}^* - \mathbf{s}^1)$. The elastic–plastic constitutive relation based on $\bar{\mathbf{n}}$ sets $(\mathbf{s}^* - \mathbf{s}^1)$ normal to $\bar{\mathbf{n}}$,

$$(\mathbf{s}^* - \mathbf{s}^1) = 2G(\mathbf{I} - \bar{\mathbf{n}}\bar{\mathbf{n}}^{\mathrm{T}})(1 - m)\,\Delta\mathbf{e}^{\mathrm{est}}. \tag{24}$$

Adding $2\mathbf{s}^1$ to both sides of Eq. (24) and recognizing that $2\mathbf{s}^1 + 2G(1 - m)\,\Delta\mathbf{e}^{\mathrm{est}}$ is parallel to $\bar{\mathbf{n}}$ by definition, we see that $(\mathbf{s}^* + \mathbf{s}^1)$ is parallel to $\bar{\mathbf{n}}$, and hence Eq. (23) is satisfied.

4.2. Element Design

Three types of finite elements were used in the analysis. For elastic solutions the $r^{-1/2}$ singular element [25] was used nearest the crack tip with arbitrary quadrilateral four-node isoparametric elements over the remainder of the configuration. To study plastic effects at the crack tip, a new singular element was designed, similar to that of Levy *et al.* [37], which has a $1/r$ shear strain singularity (with a bounded dilatational strain) and a uniform strain as admissible deformations.

The singularity elements have the shape of isosceles triangles and are focused along radial lines into the crack tip. However, they are treated as degenerate isosceles trapezoids in the sense that four nodes are assigned to the elements, one at each vertex, even though two of the nodes coincide at the crack tip. Levy *et al.* [37] introduced this coincident node technique to study the crack tip displacement variation. Contrary to their procedure, however, the coincident nodes were here constrained to move as a single point in obtaining the elastic response of the cracked body, since the nonunique crack tip displacement is a plasticity effect.

The variation of stress and hence constitutive relation in the plastic case within elements was accounted for in the following approximate manner. Each near-tip element was viewed as the composite of three subelements, each extending one-third of the height of the element. The area average strain of an individual sub-element was used in evaluating the stress state and constitutive matrix representative of the subelement. The three subelement stiffnesses were then formed and added to obtain the total element stiffness matrix. For the adjoining isoparametric elements the midpoint strain was judged adequate to calculate the stress representative of the entire element.

To obtain elastic–plastic solutions the procedure was to specify the $r^{-1/2}$ element just up to the load necessary to yield one of the subelements. Thereupon the r^{-1} element was used with its associated nonunique crack tip displacement capability. Clearly the elastic singularity implies yielding under infinitesimal load so that there is some error involved in the plastic solution by specifying the $r^{-1/2}$ near tip strain distribution up to finite loads. Actually for the size element used at the tip this error should be very small. In the round bar problem the near tip element extended a distance $\frac{1}{72}$ of the crack length, a distance at which the singularity is expected to dominate. Using the area average strain basis the first subelement yields when the strain at $\frac{3}{16} \times \frac{1}{72} \times$ crack length satisfies yield. The neglect of plasticity in the analysis until this load level should have a minor effect on the solution away from the tip at this load and as loading proceeds, the crack tip solution should show little evidence of this numerical transition procedure.

The interpolation functions used are most easily described in terms of the natural coordinates of the elements. Taking the element edges as coordinate lines $\xi = 0, 1$ and $\eta = 0, 1$ with the nodes I, J, K, L at the intersections we have the following correspondence with the physical coordinates:

$$\mathbf{x} = \mathbf{x}^I(1-\xi)\eta + \mathbf{x}^J(1-\xi)(1-\eta) + \mathbf{x}^K\xi(1-\eta) + \mathbf{x}^L\xi\eta \tag{25}$$

Equation (25) may be thought of as a mapping of the physical region onto a unit square in the (ξ, η) plane. For instance Fig. 4 illustrates the map of a near-tip element of angular extent 2α and height s_0. Notice that the edge

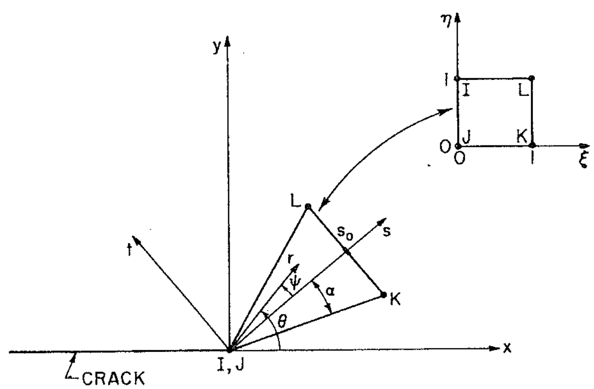

Fig. 4. Typical near crack tip element.

$\xi = 0$ with two distinct nodes I and J maps onto one point—the crack tip—in the (x, y) plane so that in this case $\mathbf{x}^I = \mathbf{x}^J$. The inverse map of this particular element in terms of the local Cartesian coordinates (s, t) and local polar coordinates (r, ψ) is

$$\xi = s/s_0, \qquad \eta = (\tan\psi/\tan\alpha + 1)/2 \tag{26}$$

The elastic singularity element has the interpolation function

$$\mathbf{u} = \mathbf{u}^{IJ}(1-\sqrt{\xi}) + \mathbf{u}^K(1-\eta)\sqrt{\xi} + \mathbf{u}^L\eta\sqrt{\xi} \tag{27}$$

The unique displacement of the crack tip nodes I and J is denoted by $\mathbf{u}^{IJ}$. From Eq. (26) we see that this displacement distribution corresponds to the expected form of $\sqrt{r}$ times a smooth function of angle. Along the edges $\eta = 0, 1$ displacement is a two-parameter function of $\xi(a + b\sqrt{\xi})$ so that there is displacement compatibility across them. Along the $\xi = 1$ edge the

displacement is linearly interpolated between $\mathbf{u}^K$ and $\mathbf{u}^L$ so that there is complete inter-element compatibility when four node isoparametric elements are joined there. When the nodes are denoted as K, L, M, N the latter element has the form

$$\mathbf{u} = \mathbf{u}^L(1-\xi)\eta + \mathbf{u}^K(1-\xi)(1-\eta) + \mathbf{u}^M\xi(1-\eta) + \mathbf{u}^N\xi\eta \tag{28}$$

The plastic singularity element interpolation function was derived through consideration of displacement distributions which correspond to a $1/r$ shear-strain singularity and importantly also a bounded dilatational strain. Levy *et al.* [37], in treating the small-scale-yielding problem, used a bilinear polar coordinate interpolation function for near tip pie-shaped elements which allowed a $1/r$ singularity in $\varepsilon_{\theta\theta}$ as well as $\varepsilon_{r\theta}$, leaving it to the numerical solution to choose a bounded $\varepsilon_{\theta\theta}$. However, it is impossible with their element to make the $1/r$ part of $\varepsilon_{\theta\theta}$ vanish for all θ. Here the dilatation boundedness condition Eq. (17) is precisely satisfied throughout the near tip elements. In the notation of Fig. 4 the condition met by the displacement components $u_s(\xi, \eta)$ and $u_t(\xi, \eta)$ is

$$\partial u_t(0, \eta)/\partial\eta = \tan\psi\, \partial u_s(0, \eta)/\partial\eta \tag{29}$$

The $1/r$ shear singularity results for any assumed displacement function which allows a crack tip displacement variation, as in the general discussion of the last section.

Only the displacements $(u_s{}^I, u_s{}^I)$ and $(u_s{}^J, u_t{}^J)$ of the nodes at (0, 1) and (0, 0) enter in the displacement distribution along $\xi = 0$ in the present formulation. Hence these degrees of freedom completely determine the strength of the shear singularity within the element as seen from the first of Eqs. (20) rewritten in present notation,

$$R(\psi) = \frac{G}{\tau_0 \cos\psi} \frac{\partial u_s(0, \eta)}{\partial \eta} \frac{d\eta}{d\psi} \tag{30}$$

With no attempt to enforce continuity of $R(\psi)$ at element boundaries $u_s(0, \eta)$ was chosen linear in η so that, to first order in ψ, $R(\psi)$ would be constant within an element,

$$u_s(0, \eta) = u_s{}^J + (u_s{}^I - u_s{}^J)\eta \tag{31}$$

Equations (29) and (31) then establish $u_t(0, \eta)$ to within a constant which in turn is determined from the end conditions $u_t(0, 1) = u_t{}^I$ and $u_t(0, 0) = u_t{}^J$. We find the distribution

$$u_t(0, \eta) = u_t^{IJ} + \tan\alpha(u_s{}^I - u_s{}^J)\eta(\eta - 1) \tag{32}$$

which has the displacement components $u_t{}^I$ and $u_t{}^J$ equal to each other and commonly called u_t^{IJ}. This constraint $u_t{}^I = u_t{}^J$ is consistent with the intuitive feeling that the shear singularity is governed mostly by a u_s displacement variation. The exact expression for $R(\psi)$ is

$$R(\psi) = \frac{G}{\tau_0 \cos^3 \psi} \frac{u_s^I - u_s^J}{2 \tan \alpha} \tag{33}$$

This is recognized as a first-order finite difference approximation to $R(\psi)$ expressed either as we have earlier or as [20] $G/\tau_0[\partial u_r(0, \psi)/\partial\psi - u_\psi(0, \psi)]$ when the displacement u_s is transformed to polar coordinates and the equation is linearized in its angular dependence.

A bilinear displacement variation throughout the element due to displacement of nodes K and L was specified. Also the distributions (31) and (32) were weighted in the ξ direction by the factor $(1 - \xi)$. The complete interpolation function for the shear singularity element is then given by

$$\begin{aligned} u_s &= \frac{u_s^I + u_s^J}{2}(1 - \xi) + [u_s^L\eta + u_s^K(1 - \eta)]\xi + \frac{u_s^I - u_s^J}{2}(2\eta - 1)(1 - \xi) \\ u_t &= u_t^{IJ}(1 - \xi) + [u_t^L\eta + u_t^K(1 - \eta)]\xi + \tan\alpha(u_s^I - u_s^J)\eta(\eta - 1)(1 - \xi) \end{aligned} \tag{34}$$

If the two coincident nodes move as one, so that $u_s^I = u_s^J$, the element is nothing more than the conventional constant strain triangle. Hence the possibility of strain free rigid body motion of the element is present. The interelement displacement compatibility condition is satisfied since displacement varies linearly on all interelement edges.

A 9-point numerical integration of the element stiffness matrices was performed. The integration stations were at $\xi, \eta = \frac{1}{6}, \frac{1}{2}, \frac{5}{6}$ and each station was weighted by $\frac{1}{9}$ of the area of the element. In the fan regions expected at the crack tip there is no angular variation in deviatoric stress state when reference is to a polar coordinate system. Thus to enhance the accuracy of using subelement area average strains to evaluate the stress of the subelement, the stresses and strains of the near tip elements, which follow from Eq. (34), were referred to polar coordinates.

4.3. Computing Details

A version of the general-purpose finite-element program MARC4 was used in this work. Calculations were done on the Brown University IBM 360/67 in double precision arithmetic. The master stiffness equations were solved by direct elimination. The shear singularity element formulation required double precision; single precision calculations resulted in very erratic strain distributions. Experience with other formulations in single precision using isoparametric or polar elements (and the $r^{-1/2}$ singular element in the elastic case) gave no similar direct hint of arithmetic precision

difficulties, establishing the shear singularity formulation as particularly sensitive to computational mode.

4.4. Small Scale Yielding Results

The problem under consideration is the plane strain contained yielding of an elastic–plastic plane with a semi-infinite edge crack under the boundary condition that the singular field of the elastic solution, Eqs. (1) and (4), is asymptotically approached as $r \to \infty$. This boundary layer formulation was proposed by Rice [20] for the analysis of sharply cracked bodies with a crack tip plastic zone which is small compared to significant configuration dimensions. The finite-element model involved a finite region about the crack with a near-tip element dimension chosen small compared to region size so that the outer boundary could effectively be considered at infinity. The displacement field (4) was imposed at the nodes on the outer edge with K as the loading parameter. Taking advantage of symmetry, only the upper half of the region ($y \geqslant 0$, using the coordinates of Fig. 1) was treated. Ahead of the crack on $y = 0$ the displacement component u_y and the shear traction were zero.

The mesh was composed of four rings of 7.5° focussed isosceles trapezoids followed by eight rings of 15° elements making a total of 192 elements and 229 nodes. The nodes described arcs of radius

$$r = 0, 0.5, 1, 1.625, 1.5^2, 2^2, \ldots, 5.5^2$$

The nodes on $r = 2.25$ not common to the adjacent 7.5° and 15° elements were constrained to maintain interelement compatibility.

The plastic solution was obtained by specifying successive increments in K equal to 25% of K_0—the stress intensity factor which causes the first subelement to yield. At each load increment the solution was the result of three iterations on the representative element constitutive matrices. Loading ceased when elements of the fifth ring yielded so that the extent of the plastic zone was always small compared to the outer radius.

From the exact elastic distribution (1) we find that initial yield occurs at an angle of $\cos^{-1}[(1 - 2\nu)^2/3] \approx 87°$, for $\nu = 0.3$. Furthermore, K_0 for yielding a radius r_y can be determined from $K_0/\sigma_0(2\pi r_y)^{1/2} = 1.10$ for this Poisson ratio. In this problem subelement yielding was based on the subelement midpoint stress so that r_y was $\frac{1}{12}$. The element between 82.5° and 90° yielded first; the midpoint angle being 86.25° indicates excellent finite-element agreement with the theoretical value. The finite element yield load parameter $K_0/\sigma_0(2\pi r_y)^{1/2}$ was 1.07—less than 3% deviation from theory. The angular near tip stress variation was also in excellent agreement.

The crack tip opening displacement [twice the y component of displacement of the node at $(0, \pi)$] made dimensionless by the similarity parameter $K^2/E\sigma_0$ is plotted in Fig. 5 as a function of K/K_0. From dimensional considerations $\delta_t/(K^2/E\sigma_0)$ is constant but because of the numerical procedure the value varies with K/K_0 until the near tip plastic field is established. A

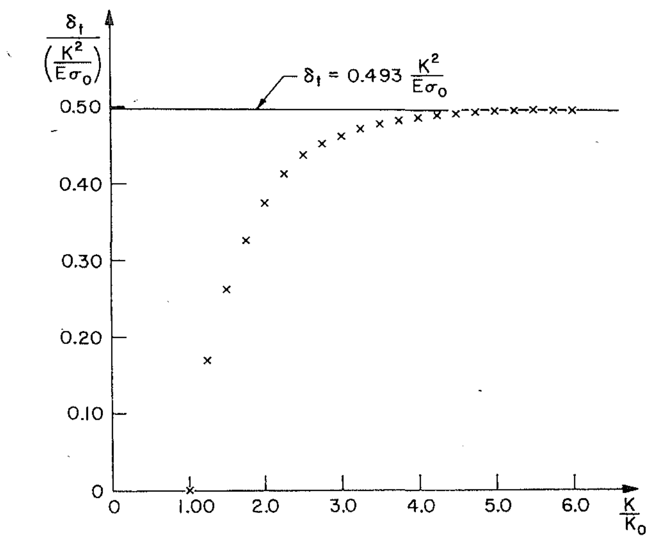

Fig. 5. Dimensionless crack tip opening displacement $\delta_t/(K^2/E\sigma_0)$ versus loading parameter K/K_0 for small-scale-yielding problem.

value of 0.493 was achieved at $K/K_0 = 4.75$ and it did not change for the remainder of the loading so that we conclude that for small-scale yielding

$$\delta_t = 0.493\, K^2/E\sigma_0 \tag{35}$$

Levy *et al.* [37] found a factor of 0.425 from their incremental plasticity finite element results. The current estimate is thought more accurate since their polar element involved a dilatational singularity along with the expected shear singularity. With the physically less precise deformation theory of plasticity the J integral can be used to estimate the factor: Assuming an $R(\theta)$ symmetrical about $\theta = 90°$ Rice [20] predicted a factor of 0.613. Using $R(\theta)$ from the nonhardening limit of the power law hardening singularity Rice and Johnson [39] showed that the resulting value was 0.717.

The crack tip stress field as represented by the stresses of the twenty-four subelements nearest the crack tip approaches a distribution similar to the

Prandtl field that was discussed in the last section. The progression of $\sigma_{r\theta}(\theta)/\sigma_0$ from the elastic distribution ($K/K_0 = 1$) to the fully developed distribution ($K/K_0 > 4.5$) which is plotted in Fig. 6 is typical of all the stress components. The most obvious connection between the solution and the Prandtl field is that both have distinct fans in the range $45° < \theta < 135°$.

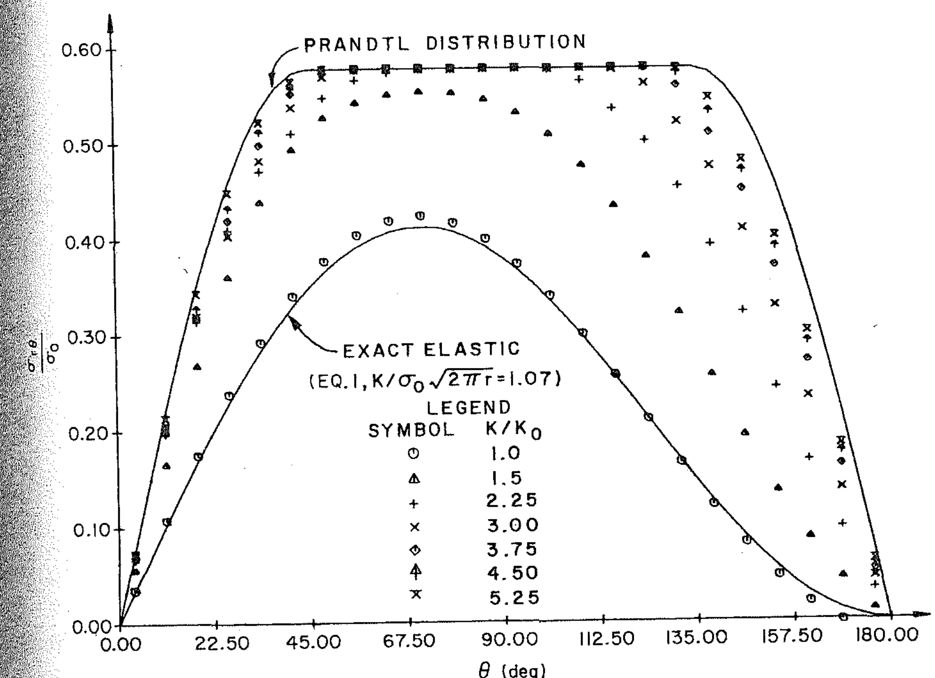

Fig. 6. Crack tip shear stress distribution at various load steps for the small scale yielding problem.

Also the stress $\sigma_{\theta\theta}$ of the subelement in the range $0 < \theta < 7.5°$ reaches the value $2.96\sigma_0$ at $K/K_0 = 5.25$ which certainly is in excellent agreement with the Prandtl value of 2.97 for $\sigma_{\theta\theta}(0, 0)$. Two important assumptions used in deriving the Prandtl field were that yielding completely surrounds the crack tip and that the out-of-plane deviatoric stress s_{zz} vanishes at all values of θ. Neither condition was met in the finite element solution. The two elements between 165° and 180° remain elastic throughout the loading and $s_{zz} = 0$ only in the fan. Hence it is not surprising that the stress distributions of the Prandtl constant state region were not realized in detail. Yet from the fan results this problem does indeed show the value of using analytical work to guide in the design of numerical procedure.

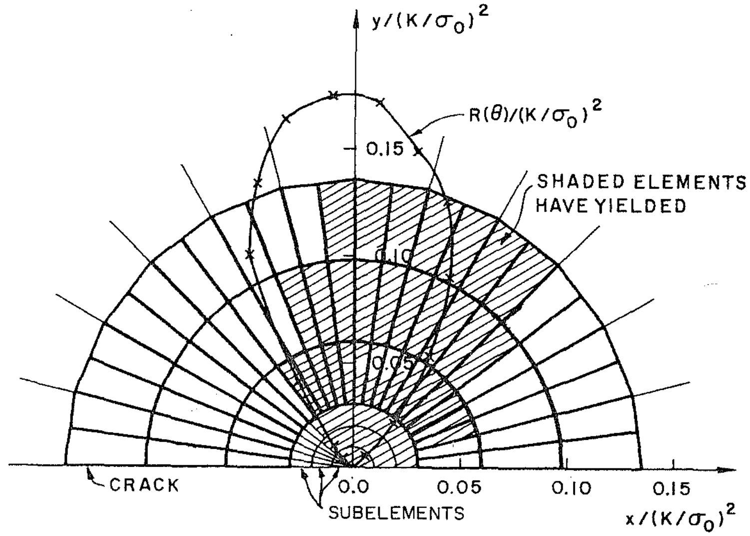

Fig. 7. Strength $R(\theta)$ of the $1/r$ shear singularity and plastic zone extent in terms of similarity coordinates $(x, y)/(K/\sigma_0)^2$, for small scale yielding.

Fig. 7 shows the near tip mesh, yielded elements and the strength $R(\theta)$ of the shear strain singularity, from the solution at $K/K_0 = 5.25$, all referred to the similarity coordinates $(x, y)/(K/\sigma_0)^2$. The contour defined by the yielded elements does not precisely define the elastic–plastic boundary due to stress variation within elements. By interpolation between load steps we find that $r_{P,\max}$, the maximum linear extent of the elastic–plastic boundary, is $0.152(K/\sigma_0)^2$ and this is at $\theta = 71°$. The boundary crosses the $\theta = 0$ line at a radius $r_{P,0} = 0.041(K/\sigma_0)^2$. The strength $R(\theta)$ was determined from the crack tip nodal displacements in accord with Eq. (33) (with $\psi = 0$). The function peaks in the range 90°–97.5° with a value

$$R_{\max} = 0.177(K/\sigma_0)^2 \tag{36}$$

In comparison, Levy *et al.* [37] found factors of 0.157, 0.036, and 0.155 for $r_{P,\max}$, $r_{P,0}$, and $R_{\max}$, respectively. The vanishingly small value of R outside of the angular range $45° < \theta < 135°$ clearly defines this range as the fan region active in the blunting of the crack tip.

4.5. Circumferentially Cracked Round Bar

The axisymmetric round bar considered has a circumferential crack penetrating its outer surface to a depth of $\frac{1}{2}$ the bar radius and a length of $4D$, where D is the bar diameter. The boundary condition was that the ends of the

bar move uniformly in the axial direction with zero shear tractions. The length was sufficient to have a uniform axial stress state at the ends during the entire loading sequence. A mesh with 384 nodes and 340 axisymmetric ring elements was used to represent the upper half of the bar which is naturally described in terms of a (ρ, z, ϕ) cylindrical coordinate system with the centerline coinciding with the z axis and the crack along $D/4 \leqslant \rho \leqslant D/2$ in each meridional plane $\phi = \text{const}$. Cross sections of the elements near the crack tip were focussed isosceles trapezoids, near the ends rectangles, and joining the two groups were arbitrary quadrilaterals. As viewed on a meridional plane there were 13 rings of 7.5° trapezoids encircling the crack tip, as for the previous small scale yielding solution. Introducing an (r, θ) polar coordinate system in this plane (with the crack along $\theta = \pm\pi$) the nodes of the trapezoids describe arcs of radius

$$r = (D/288)(0, 1, 1.5^2, 2^2, 2.5^2, 3^2, 4^2, 5^2, 6^2, 48, 60, 72, 91, 120)$$

The stress intensity factor for this geometry as a function of net section stress σ_{net} and diameter D was found by Bueckner [40] to be within one percent of $0.240\sigma_{\text{net}}(\pi D)^{1/2}$. The nodal displacements at $r/D = \frac{1}{288}$ and σ_{net} from the elastic solution were used in conjunction with the theoretical plane strain near tip field (4) to estimate K; however, nodes within 37.5° of the crack were not considered for, in this range, $\varepsilon_{\phi\phi}$ was of the same order of magnitude as the in-plane strains. A simple average of the discrete estimates of K results in a factor of 0.244 which is within 2% of Bueckner's solution. The stress σ_{zz} of the subelement between $0 < \theta < 7.5°$ corresponds to 0.247 which is 3% from Bueckner.

The accuracy of the partial-stiffness treatment, Eq. (21), of elements making the elastic to elastic–plastic transition within a load increment and the rate of convergence of the mean yield surface normal technique are greatly affected by the size of the load increment. A successful procedure in terms of convergence rate involved regulating the load increment so that only elements within 10% of yield would yield during an increment, and also allowing three iterations for each increment. For small scale yield the sufficient load step sizes were prejudged by assuming that the elastic regions responded proportionally to load up to yield. The displacement of the end of the bar was increased to 38.2 times the end displacement $(u_z^{\text{end}})_0$ at first yield in 42 increments in the following manner

2 steps of $0.1(u_z^{\text{end}})_0$, 6 of 0.2, 3 of 0.3, 3 of 0.4, 2 of 0.5, 6 of 0.7, 9 of 1.0, 7 of 1.5, 4 of 2.25

The load-deflection curve, $\sigma_{\text{net}}/\sigma_0$ versus $Eu_z^{\text{end}}/\sigma_0 D$, is presented in Fig. 8. The end displacement was increased until the limiting elastic–plastic zone

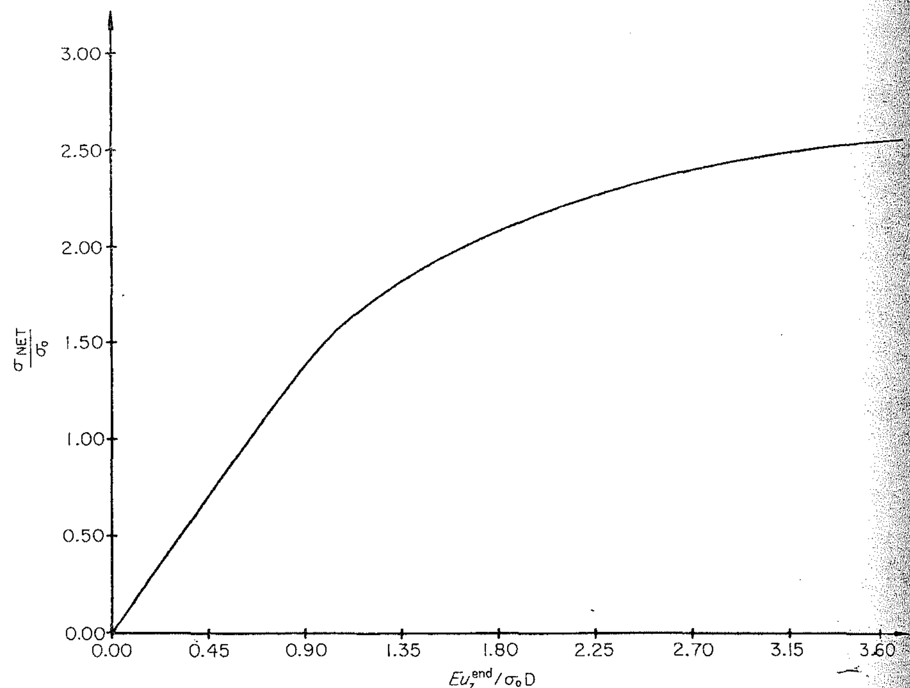

Fig. 8. Load deflection curve for round bar.

was achieved. The corresponding limit stress for this Mises idealization is $\sigma_{net} \cong 2.56\sigma_0$. In comparison, Shield [41] found a limit pressure of $5.69\tau_0$ for axisymmetric frictionless indentation of an elastically rigid–perfectly-plastic Tresca half-space. While the flow was confined to a radius of 1.58 times the punch radius in Shield's problem, the present finite-element result is that yielding spreads to include the outside surface of the bar at limit load. Figure 9 shows the yielded regions at different stages of loading. If the plasticity had been confined to the bar interior Shield's limit load could serve to establish bounds to the Mises limit load for the crack depth chosen by invoking corollaries to the limit theorems of plasticity.

When the Mises and Tresca materials are assigned identical shear limits the ratio of the finite-element limit stress to Shield's is $4.43/5.69 = 0.78$; when matched in tension the ratio is $2.56/2.85 = 0.90$. Figure 10 is a plot of the two net section stress distributions, σ_{zz}/σ_0 versus $4\rho/D$ at $z = 0$, at limit load. The larger Tresca stresses over most of the section can be explained in terms of the factor of 0.9 between the Mises and Tresca limit loads. The Tresca curve monotonically decreases from a centerline value of $3.60\sigma_0$ to $2.57\sigma_0$ while the Mises curve increases from $2.10\sigma_0$ to $3.05\sigma_0$ at the crack tip (or

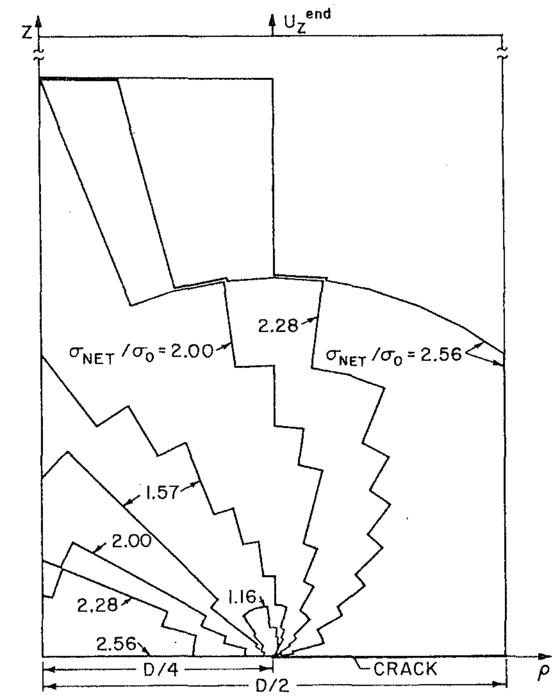

Fig. 9. Round bar yield zones at various load levels.

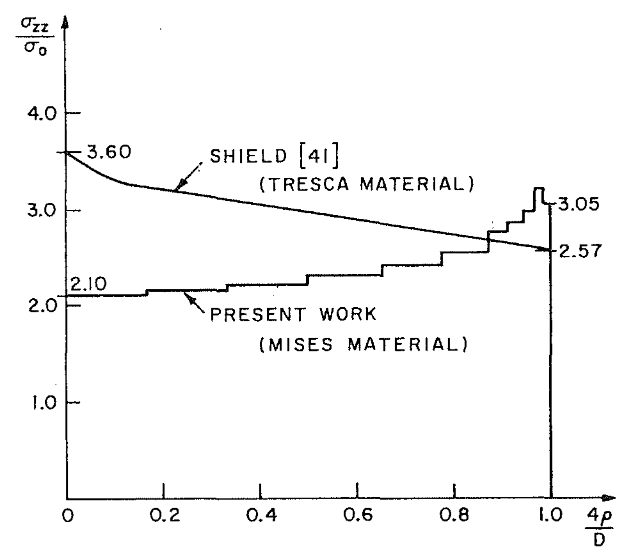

Fig. 10. Round bar net section stress distribution at limit load.

punch surface in Shield's context) when averaging the near tip subelement values of 2.94, 2.98, and 3.23.

The crack tip small scale yielding solution was essentially that of the previous asymptotic problem. As explained, the normalized crack tip opening displacement $\delta_t/(K^2/E\sigma_0)$ increases from value zero to a characteristic small scale yielding value over a small initial load range due to numerical procedure. Also, once the plastic zone extends to an appreciable fraction of crack length $\delta_t/(K^2/E\sigma_0)$ dramatically increases with K signaling the beginning of "large scale" yielding. The value of $\delta_t/(K^2/E\sigma_0)$ increased to within 10% of the asymptotic solution value 0.493 at the eighth load increment corresponding to $\sigma_{net}/\sigma_0 = 0.37$ and the plasticity was confined to the first ring of elements about the crack tip. The value was 10% higher than the asymptotic solution at $\sigma_{net}/\sigma_0 = 0.85$ and at this state plasticity was confined to a radius of $D/32$. This plastic zone size could be used to set a rough upper limit to the applicability of linear fracture mechanics treatment of crack tip plasticity.

The function $R(\theta)$ in the small-scale yielding range differed slightly from the distribution for the asymptotic problem in that the function peaked between 82.5° and 90°; in the former solution R_{max} was in the range 90° to 97.5°. This

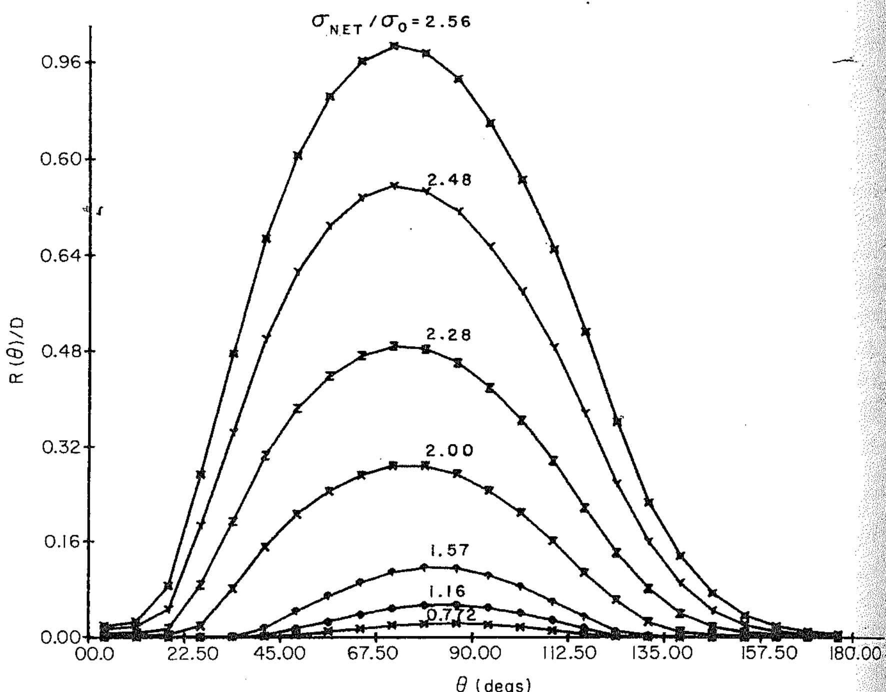

Fig. 11. Strength $R(\theta)$ of $1/r$ shear singularity for round bar at different stages of loading.

is most likely the influence of the centerline which is felt due to the relatively coarse mesh of the present problem. In Fig. 11 $R(\theta)/D$ is plotted for various load states in the large scale yielding range. In conjunction with the elastic–plastic zones of Fig. 9, one can see that R serves as a reasonable estimate to the extent of the plastic zone at angles which are within the $1/r$ shear fan while the plastic zone at the angle remains interior to the specimen boundaries. As loading progresses the fan region extends from the Prandtl range of $45° < \theta < 135°$ to the larger range of $15° < \theta < 157.5°$. This may, however, reflect a failure of the numerical solution to accurately meet the stress-free crack surface boundary condition in the innermost element as fully plastic conditions are reached.

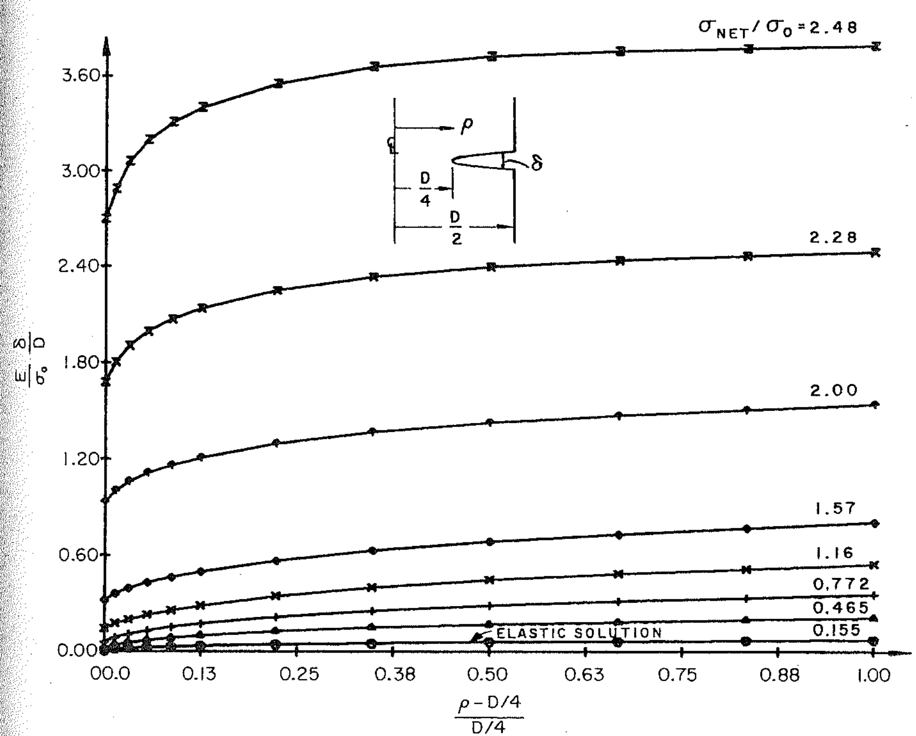

Fig. 12. Round bar crack profile at various load levels.

Figure 12 is a plot of the opening displacement δ of the neighboring points on the crack surfaces, as a function of distance from the crack tip, for various net stress levels. It is clear from these curves that, throughout the large-scale-yielding range, the crack tip opening displacement, δ_t ($=\delta$ at $\rho = D/4$) is very significant even when compared to the flank opening δ at $\rho = D/2$.

These results may be helpful in correlating large scale yield fractures of this geometry since if fracture is controlled by a critical crack tip state, it is quite likely reflected in the attainment of a critical crack opening displacement, at least for cases such as the present for which the stress triaxiality does not vary appreciably from small scale to general yielding conditions.

5. Three-Dimensional Problems

Both structural applications of fracture mechanics and the interpretation of experimental results require advances in three-dimensional stress analysis. Work to date has been limited, and has focused on the stress analysis of part-through-the-thickness surface cracks in the walls of plate or shell structures, as representative of flaw types in applications, and on the transition from plane strain to plane stresslike constraint near the tip of a straight through-the-thickness crack in a plate. This last problem is, of course, important to the interpretation of fracture test results which are typically obtained on plate specimens precracked in this way. It is also of interest for the information it sheds on the actual three-dimensional aspects of what is commonly treated as a two-dimensional problem.

5.1. Through Crack in a Plate

The straight, through-the-thickness crack in a plate has been studied by Aryes [42] using finite difference methods, by Cruse [15] and Cruse and Van Buren [16] using a numerical solution of singular integral equations over the specimen boundary, and by Levy *et al.* [43] using finite-element methods. Only Ayres gave results for this problem in the plastic range, but he made no special provisions beyond mesh refinement for attaining near tip accuracy. Levy *et al.* employed a singular element similar to that of their earlier plane strain study [37] and to that of the last section, with layers of polar arrays of the elements being stacked through the plate thickness.

Figure 13 is replotted from Cruse's [15] results on a compact ($2h \times 2h \times h$, where h is plate thickness) fracture test specimen containing an edge crack of length h which is wedged open by end forces. Lines of constant value for the parameter α [$=\sigma_{zz}/\nu(\sigma_{xx} + \sigma_{yy})$] are shown for half the plane of material directly ahead of the crack. The parameter is called the "degree of plane strain" since such conditions correspond to $\alpha = 1$. One sees that plane strain conditions are indeed approached at the crack tip, although the fall off toward a plane stress state ($\alpha = 0$) is quite rapid. Similar results were found by Levy *et al.* [43], who studied a circular plate of six thicknesses in radius with a through crack having its tip at the plate center. For boundary conditions they imposed the stresses σ_{rr} and $\sigma_{r\theta}$ of the charactristic $r^{-1/2}$ singularity appropriate to the two-dimensional-plane stress theory. Figure 14 shows their

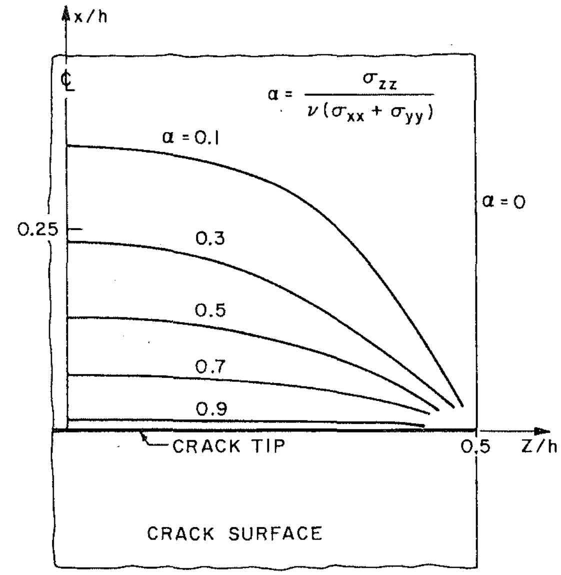

Fig. 13. Results showing the transition from plane strain to plane stress behavior near the tip of a through-the-thickness crack in an elastic plate, from Cruse [15].

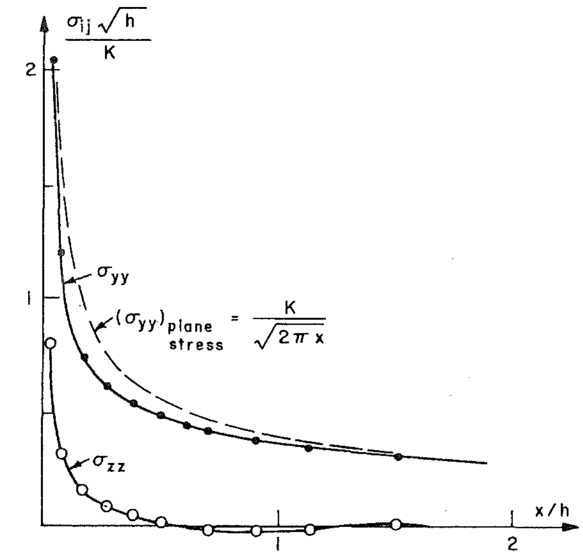

Fig. 14. Results demonstrating the rapid transition to a plane stress condition away from the crack tip in a through-the-thickness cracked elastic plate, from Levy *et al.* [43].

results for σ_{yy} and σ_{zz} on the line in the plate middle surface directly ahead of the crack. The dashed line shows the two-dimensional plane stress result for σ_{yy}. Again, the rapid approach to a plane stress state may be noted; σ_{zz} is negligible even in the middle surface beyond a distance of about a half-thickness. The last two figures tend to make plausible the rather large ratio of plate thickness to plastic zone size found necessary to assure plane strain conditions within the plastic region at fracture [44].

5.2. Surface Cracks

Several different computational approaches have also been taken for problems of part-through-the-thickness surface cracks. For example, Kobayashi and Moss [45] and Smith and Alavi [46] have employed alternating methods in three-dimensional elasticity, based on the Boussinesq solution for a half space and on that for removal of tractions from an embedded circular or elliptical shaped crack in an infinite body, to estimate K for circular arc and semielliptical surface cracks in plates. The papers by Ayres [42] and Levy *et al.* [43] employing finite difference and isoparametric finite-element formulations, respectively, have discussed the elastic and elastic–plastic fields near a semielliptical surface crack in a plate.

Also, Rice and Levy [47] have developed a model for problems of long surface cracks (in comparison to plate thickness) which reduces these to problems in the two-dimensional theory of plane stress and bending for a plate containing a line spring which represents the part-cracked section. Their original work reduced the problem to two coupled integral equations, solved numerically, for the force and moment transmitted across the line spring. However [48], the model has been extended to cracks in shells, and a finite-element formulation has been developed for incorporation in existing two-dimensional plate and shell programs. Results for K have been given for surface cracks of various shapes in plates, and for axial and circumferential semielliptical cracks in the wall of a cylindrical tube. Their model shows promise of extension to the plastic range, and to application within shell analysis programs to a variety of surface crack locations in pressure vessels.

6. Micromechanics and Development of Fracture Criteria

Here we discuss the use of computational methods in the description of fracture processes on the microscale, and in the merging of such studies with elastic–plastic analyses at the continuum level so as to develop rational fracture criteria. The area is not yet very much studied, and hence our emphasis will be in part on pointing out what we consider to be opportunities for productive use of computational stress analysis methods for problems of this type. These include the effects of plastic flow, finite strains, and deformation instabilities.

6.1. Ductile Fracture Mechanisms

Fracture mechanisms in structural metals, apart from low-temperature cleavage in steels, generally involve substantial plastic flow on the microscale. This arises through the formation of small voids, typically by the decohesion or cracking of hard inclusion particles, which undergo large ductile expansion until final separation results from coalescence of arrays of these voids. That is, fracture arises as a kinematic result of large plastic flow. This is so even for materials such as the high-strength steels and aluminum alloys which may, under plane strain conditions, show macroscopically brittle crack advance with plastic zone sizes in the millimeter range. On a scale of, say, 5 to 100 μm the resulting fracture surfaces show evidence of great ductility with local strains on the order of unity. McClintock [3, 38, 49] has discussed this fracture mechanism in detail. He and Rice and Tracey [50] have applied continuum plasticity solutions for cavity expansion as models for hole growth.

In general, however, the modeling of void growth should include a treatment of finite shape changes, interactions between neighboring voids, and the possibly unstable coalescence of neighboring voids or void arrays. This necessarily involves numerical formulations for large deformations, of the type presented, for example, by Hibbit *et al.* [51] and Needleman [52]. In fact, Needleman's paper contains a finite-element solution for the large ductile expansion of a periodic array of initially cylindrical holes in a power law hardening material. His procedure was based on a form for the incremental constitutive law at finite strain proposed by Budiansky [53]. This is consistent with a variational principle for the rate problem, as in the small distortion theory, and the finite-element method was based directly on it. In contrast, Hibbitt *et al.* propose a constitutive law in which the Jaumann stress rate is employed, rather than Budiansky's time derivative of a stress measure referred to convected coordinates, and no variational principle is then applicable. The formulation begins instead directly from the principle of virtual work and the resulting statement of equilibrium is differentiated to derive the governing finite-element equations of the rate problem.

Computations of the type done by Needleman also serve to predict the slight dilatation which should appear in macroscopic plastic constitutive laws as a consequence of void growth. Berg [54] has suggested that such dilatational constitutive laws could be used as a basis for stress analysis procedures which include ductile fracture initiation as a *consequence* of a proper stress analysis, rather than as an ad hoc supplement to such an analysis.

Here the idea is that such constitutive laws, which already include the volume change due to void growth, may also ultimately permit localization in a band as representative of unstable void coalescence on the microscale. This may occur when the hardening in an increment of deformation is just balanced by the softening due to the increased porosity through void growth, provided also that the kinematic condition is met of existence of a plane of zero extension rates. The types of problems for which such an approach may be valuable (e.g., metal-forming processes) typically involve extensive plastic flow and will require a numerical formulation appropriate to finite strain. Very little has been done to date. Indeed, even the classic problem of ductile fracture initiation in the necked region of a round tensile bar is unsolved at present.

The mechanics of void initiation from inclusions has also received little attention, although the problem of determining the stress state in and near a nonyielding inclusion in a ductile matrix is certainly within the capability of existing analysis methods. Huang [55] has presented such a study for a circular cylindrical inclusion in a Ramberg–Osgood power hardening material through a method of Fourier expansion and finite differences which, unfortunately, does not seem to offer the possibility of general application.

6.2. Fracture Mechanisms at a Crack Tip

The elastic–plastic crack stress analyses discussed elsewhere in this paper were based on conventional small strain-analysis procedures, in that effects of geometry changes on the governing equations were neglected. This is obviously incorrect within a distance from the tip comparable in size to the predicted opening displacement. Analysis at such a scale is important since ductile fracture mechanisms are operative in this very near tip region where large strains occur.

Rice and Johnson [39] have shown how the solutions based on neglect of geometry changes may be employed to set boundary conditions on a localized analysis of the large crack tip deformations for the nonhardening model. In this case it is important that the distribution $R(\theta)$ of the strength of the strain singularity be known (as, for example, in Figs. 7 and 11), for from it the crack tip velocity field is computed and this is the boundary condition for the local large-strain analysis. The analysis is based on the application of slip line theory to the near tip region, and McClintock [3, 56] has similarly discussed large geometry changes at the tip.

When the tip is drawn as progessively blunted by increasing load as in Fig. 15, the constant stress regions A and B as in the Prandtl field of Fig. 2 remain, but they are separated by a fan of straight slip lines C which is no longer centered. Instead it feeds into a spiral region D ahead of the tip of a size roughly comparable to the crack opening. We have seen that δ_t is of the order of an initial yield strain times the maximum linear dimension of the plastic zone. Representative numerical values for a wide range of low and high strength structural metals are between 0.003 and 0.03 times the zone size. Hence, in Fig. 15 we see a minute fraction of the total plastic region and, indeed, the blunted tip would appear essentially as a point when viewed on the size scale of the plastic zone. For this reason, Rice and Johnson suggested that crack tip blunting could be studied for the contained plastic yielding range by applying rigid–plastic theory locally to region D, using the fact that straight slip lines of the fan transmit a uniform velocity along their length and hence that radial velocity, as a function of angle, should differ negligibly from the result for the solution which neglects geometry change effects. That is, the radial displacement rate $\dot{u}_r^{0}(\theta)$ from solutions of the type discussed earlier is taken as the normal velocity, as a function of slip line angle, imposed from the fan region along the boundary between C and D. From this it is straightforward to numerically calculate, in order, the velocity field in terms of slip line coordinates, the movement of the crack tip, the resulting physical coordinates of points of the slip line field in D, and hence the entire local strain and displacement solution for crack tip blunting. Rice and Johnson describe a computational scheme for doing this and give some representative results.

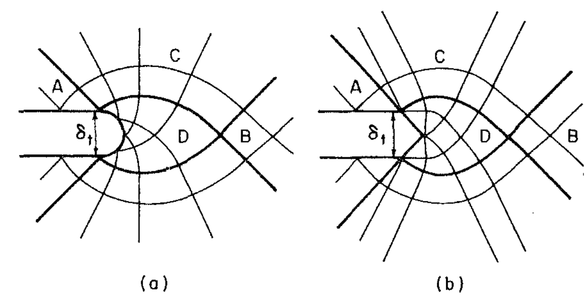

Fig. 15. Two possible solutions to the slip line analysis of the blunting of an initially sharp-tipped crack.

The greatest difficulty with such solutions is illustrated in Fig. 15: As McClintock [3] has emphasized, solutions for an initially sharp crack are nonunique. It is possible to find a solution involving smooth blunting as in (a); it is also possible to find solutions in which the crack tip retains sharp corners of singular strain rate as in (b). Indeed, there appears to be nothing in continuum plasticity to enable a choice. McClintock suggests from observations of fracture surfaces that the latter is the more realistic picture.

Strain-hardening effects cannot be properly included in the slip line analysis of blunting. Nor can the interactive effects of growing voids. Hence, it would seem desirable to apply some of the numerical methods for finite strain to the crack tip blunting case. The problem is not straightforward, however, due to the extremely small size of the large strain region in comparison to plastic zone dimensions (or, equivalently, to the great strain gradients involved), and to the nonuniqueness as illustrated by Fig. 15.

As we have noted earlier, very little work has been done on cracks which advance in a quasi-static fashion under increasing load. Of course, near tip accuracy is paramount in this case as always when fracture prediction is a goal of the numerical solution. Perhaps a finite-element treatment could be based on a focused mesh which moves relative to the material in each increment. Also, it would seem necessary that some plausible model of crack advance at the microstructural level be analyzed in parallel with the continuum calculations in this case, for otherwise the increment in crack length accompanying a given increment in load is not determined. McClintock [3, 38] has suggested that a decohering layer ahead of the crack may provide a proper model. The layer is imagined to represent a region of material in which void growth is already in its unstable stages, so that a falling stress versus separation-distance relation applies as a boundary condition on the continuum plasticity problem. The amount of crack advance due to a load increment in this formulation would correspond to that length ahead of the current crack tip across which zero load is transmitted.

Additional computational problems arise with subcritical crack growth by stress corrosion and fatigue. For the first of these, the mechanical features of the near tip state could be determined through any program suitable for quasi-static crack advance. In the case of fatigue, important computational problems include the determination of the cyclic deformation states near the tip, its progressive blunting and sharpening, and the role of interference of previously deformed material with crack closure at its tip.

7. Conclusion

Numerical procedures for accurate determination of elastic stress intensity factors for the general two-dimensional crack problem were reviewed. The elastic–perfectly-plastic crack tip deformation state was investigated through a finite element treatment which was designed to allow the $1/r$ shear singularity and associated crack tip opening displacement predicted from a detailed asymptotic study. The importance of basing crack tip numerical procedure on analytical results was emphasized when accuracy sufficient to develop fracture criteria is required.

The small scale yielding problem was modelled and expressions for crack tip opening displacement, shear singularity amplitude, and plastic zone extent were presented.

A finite-element solution to the large scale yielding of the circumferentially cracked round tension bar was presented. The global solution as reflected through the resulting limit load, net section stress distribution, yield zones, and crack profile and the local crack tip solution were discussed as relevant to fracture testing and prediction.

The three-dimensional aspects of flawed structures were discussed and numerical treatments of the subject were reviewed. Finally, ductile fracture mechanisms and specifically crack tip fracture on the microscale were discussed.

Acknowledgment

We wish to acknowledge financial support from the National Aeronautics and Space Administration under Grant NGL-40-002-080 to Brown University.

References

1. Paris, P. C., and Sih, G. C., "Stress Analysis of Cracks," in *Fracture Toughness Testing and Its Applications*, pp. 30–76. ASTM-STP-381. Philadelphia, Pennsylvania, 1965.
2. Rice, J. R., "Mathematical Analysis in the Mechanics of Fracture," in *Fracture: An Advanced Treatise* (Liebowitz, H., ed.), Vol. 2, pp. 191–311. Academic Press, New York, 1968.
3. McClintock, F. A., "Plasticity Aspects of Fracture," in *Fracture: An Advanced Treatise* (Liebowitz, H., ed.), Vol. 3, pp. 47–225. Academic Press, New York, 1971.
4. Gross, B., Srawley, J. E., and Brown, W. F., "Stress Intensity Factors for a Single Edge Notch Tensile Specimen by Boundary Collocation of a Stress Function," NASA Tech. Note D-2395 (1964).
5. Gross, B., and Srawley, J. E., "Stress Intensity Factors for Single Edge Notch Specimens in Bending or Combined Bending and Tension," NASA Tech. Note D-2603 (1965).
6. Gross, B., and Srawley, J. E., "Stress Intensity Factors for Three Point Bend Specimens by Boundary Collocation," NASA Tech. Note D-3092 (1965).
7. Kobayashi, A. S., Cherepy, R. B., and Kinsel, W. C., "A Numerical Procedure for Estimating the Stress Intensity Factor of a Crack in a Finite Plate," *J. Basic Eng.* **86**, 681–684 (1964).
8. Bowie, O. L., "Analysis of an Infinite Plate Containing Radial Cracks Originating from the Boundary of an Internal Circular Hole," *J. Math. Phys.* **35**, 60–71 (1956).
9. Bowie, O. L., "Rectangular Tensile Sheet with Symmetric Edge Cracks," *J. Appl. Mech.* **31**, 208–212 (1964).
10. Bowie, O. L., "Analysis of Edge Notches in a Semi-Infinite Region," *J. Math. Phys.* **45**, 356–366 (1966).
11. Kaminskij, A. A., "Critical Loads in Regions Weakened by Holes with Cracks," in *Kontsentratsija Naprjazhenij*, Vol. 1, pp. 130–136. Naukovaja Dumka, Kiev, 1965.

12. Bowie, O. L., and Neal, D. M., "A Modified Mapping-Collocation Technique for Accurate Calculation of Stress Intensity Factors," *Int. J. Fracture Mech.* **6**, 199–206 (1970).
13. Greif, R., and Sanders, J. L., "The Effect of a Stringer on the Stress in a Cracked Sheet," *J. Appl. Mech.* **32**, 59–66 (1965).
14. Bueckner, H. F., "Some Stress Singularities and Their Computation by Means of Integral Equations," in *Boundary Value Problems in Differential Equations* (Langer, R., ed.), pp. 215–230. Univ. of Wisconsin Press, Madison, Wisconsin, 1960.
15. Cruse, T. A., "Lateral Constraint in a Cracked Three Dimensional Elastic Body," *Int. J. Fracture Mech.* **6**, 326–328 (1970).
16. Cruse, T. A., and Buren Van, W., "Three Dimensional Elastic Stress Analysis of a Fracture Specimen with an Edge Crack," *Int. J. Fracture Mech.* **7**, 1–15 (1971).
17. Tirosh, J., "A Direct Numerical Method for Stress and Stress Intensity Factor in Arbitrary, Cracked, Elastic Bars Under Torsion and Longitudinal Shear," *J. Appl. Mech.* **37**, 971–976 (1970).
18. Chan, S. K., Tuba, I. S., and Wilson, W. K., "On the Finite Element Method in Linear Fracture Mechanics," *Eng. Fracture Mech.* **2**, 1–17 (1970).
19. Hayes, D. J., "Some Applications of Elastic Plastic Analysis to Fracture Mechanics," Ph.D. Thesis, Imperial College of Sci. and Technol. (1970).
20. Rice, J. R., "A Path Independent Integral and the Approximate Analysis of Strain Concentration by Notches and Cracks," *J. Appl. Mech.* **35**, 379–386 (1968).
21. Barone, M. A., and Robinson, A. R., "Approximate Determination of Stresses near Notches and Corners in Elastic Media by an Integral Equation Method," Univ. of Illinois Civil Eng. Stud., Struct. Res. Ser. No. 374 (1971).
22. Rice, J. R., "Some Remarks on Elastic Crack Tip Stress Fields," *Int. J. Solids Structures*, **8**, 751–758 (1972).
23. Wilson, W. K., "On Combined Mode Fracture Mechanics," Westinghouse Res. Lab., Res. Rep. 69-1E7-FMECH-R1, Pittsburgh, Pennsylvania (1969).
24. Hilton, P., and Hutchinson, J. W., "Plastic Intensity Factors for Cracked Plates," *Eng. Fracture Mech.* (in press).
25. Tracey, D. M., "Finite Elements for Determination of Crack Tip Elastic Stress Intensity Factors," *Eng. Fracture Mech.* **3**, 255–265 (1971).
26. Wilson, W. K., Plane Strain Crack Toughness Testing of High Strength Metallic Materials, ASTM-STP-410, pp. 75–76, Philadelphia, Pennsylvania, 1969.
27. Lee, C. H., and Kobayashi, S., "Elasto-plastic Analysis of Plane Strain and Axisymmetric Flat Punch Indentation by the Finite Element Method," *Int. J. Mech. Sci.* **12**, 349–370 (1970).
28. Marcal, P. V., and King, I. P., "Elastic-Plastic Analysis of Two-Dimensional Stress Systems by the Finite Element Method," *Int. J. Mech. Sci.* **9**, 143–155 (1967).
29. Swedlow, J. L., Yang, A. H., and Williams, M. L., "Elasto-Plastic Stresses and Strains in a Cracked Plate," in *Proc. Int. Conf. Fracture, 1st, Sendai, 1965* (Yokobori, T., *et al.*, eds.), Vol. I, pp. 259–282. Jap. Soc. for Strength and Fracture of Mater., Tokyo, 1966.
30. Swedlow, J. L., "Elasto-Plastic Cracked Plates in Plane Strain," *Int. J. Fracture Mech.* **5**, 33–44 (1969).
31. Wells, A. A., "Crack Opening Displacements from Elastic-Plastic Analyses of Externally Notched Tension Bars," *Eng. Fracture Mech.* **1**, 399–410 (1969).
32. Cherepanov, G. P., "Crack Propagation in Continuous Media," *Appl. Math. Mech. (PMM)* **31**, 476–488 (1967).
33. Hutchinson, J. W., "Singular Behavior at the End of a Tensile Crack in a Hardening Material," *J. Mech. Phys. Solids* **16**, 13–31 (1968).
34. Hutchinson, J. W., "Plastic Stress and Strain Fields at a Crack Tip," *J. Mech. Phys. Solids* **16**, 337–347 (1968).

35. Rice, J. R., "The Mechanics of Crack Tip Deformation and Extension by Fatigue," in *Fatigue Crack Propagation*, ASTM-STP-415, pp. 247–309 (1967).
36. Rice, J. R., and Rosengren, G. F., "Plane Strain Deformation Near a Crack Tip in a Power Law Hardening Material," *J. Mech. Phys. Solids* **16**, 1–12 (1968).
37. Levy, N., Marcal, P. V., Ostergren, W. J., and Rice, J. R., "Small Scale Yielding Near a Crack in Plane Strain: A Finite Element Analysis," *Int. J. Fracture Mech.* **7**, 143–156 (1971).
38. McClintock, F. A., "Local Criteria for Ductile Fracture," *Int. J. Fracture Mech.* **4**, 101–130 (1968).
39. Rice, J. R., and Johnson, M. A., "The Role of Large Crack Tip Geometry Changes in Plane Strain Fracture," in *Inelastic Behavior of Solids* (Kanninen, M. F., *et al.*, eds.), pp. 641–672. McGraw-Hill, New York, 1970.
40. Bueckner, H. P., "Coefficients for Computation of the Stress Intensity Factor K_I for a Notched Round Bar," in *Fracture Toughness Testing and Its Applications*, ASTM-STP-381, pp. 82–83, Philadelphia, Pennsylvania, 1965.
41. Shield, R. T., "On the Plastic Flow of Metals Under Conditions of Axial Symmetry," *Proc. Roy. Soc. Ser. A* **233**, 267–287 (1955).
42. Ayres, D. J., "A Numerical Procedure for Calculating Stress and Deformation Near a Slit in a Three Dimensional Elastic-Plastic Solid," *Eng. Fracture Mech.* **2**, 87–106 (1970).
43. Levy, N. J., Marcal, P. V., and Rice, J. R., "Progress in Three-Dimensional Elastic-Plastic Stress Analysis for Fracture Mechanics," *Nucl. Eng. Design* (in press).
44. Srawley, J. E., and Brown, W. F., "Fracture Toughness Testing," in *Fracture Toughness Testing and Its Applications*, ASTM-STP-381, pp. 133–193. Philadelphia, Pennsylvania, 1965.
45. Kobayashi, A. S., and Moss, W. L., "Stress Intensity Magnification Factors for Surface-Flawed Tension Plate and Notched Round Tension Bar," *Proc. Int. Conf. Fracture, 2nd*, Brighton, England (1968).
46. Smith, F. W., and Alavi, M. J., "Stress Intensity Factors for a Part Circular Surface Flaw," in *Pressure Vessel Technology, Part II, Materials and Fabrication*, pp. 793–800. ASME, New York, 1969.
47. Rice, J. R., and Levy, N., "The Part Through Surface Crack in an Elastic Plate," *J. Appl. Mech.* (in press) (ASME Paper No. 71-APM-20, 1971).
48. Levy, N., and Rice, J. R., "Surface Cracks in Elastic Plates and Shells," Brown Univ. Tech. Rept. NGL 40-002-080/6 to NASA, 1971.
49. McClintock, F. A., "A Criterion for Ductile Fracture by the Growth of Holes," *J. Appl. Mech.* **35**, 363–371 (1968).
50. Rice, J. R., and Tracey, D. M., "On the Ductile Enlargement of Voids in Triaxial Stress Fields," *J. Mech. Phys. Solids* **17**, 201–217 (1969).
51. Hibbitt, H. D., Marcal, P. V., and Rice, J. R., "A Finite Element Formulation for Problems of Large Strain and Large Displacement," *Int. J. Solids Struct.* **6**, 1069–1086 (1970).
52. Needleman, A., "Void Growth in an Elastic-Plastic Medium," *J. Appl. Mech.*, **39**, 964–970 (1972).
53. Budiansky, B., "Remarks on Solid and Structural Mechanics," *Problems of Hydrodynamics and Continuum Mechanics*, pp. 77–83. Soc. for Ind. and Appl. Math., Philadelphia, Pennsylvania, 1969.
54. Berg, C. A., "Plastic Dilation and Void Interaction," in *Inelastic Behavior of Solids* (Kanninen, M. F., *et al.*, eds.), pp. 171–210. McGraw-Hill, New York, 1970.
55. Huang, W.-C., "Theoretical Study of Stress Concentrations at Circular Holes and Inclusions in Strain Hardening Materials," Harvard Univ. Rep. SM-45 (1970).
56. McClintock, F. A., "Crack Growth in Fully Plastic Grooved Tensile Specimens," in *Physics of Strength and Plasticity* (Argon, A. S., ed.), pp. 307–326. M.I.T. Press, Cambridge, Massachusetts, 1969.